Progress in Oceanography 208 (2022) 102884

Contents lists available at ScienceDirect

Progress in Oceanography

journal homepage: www.elsevier.com/locate/pocean

Circulation and overturning in the eastern North Atlantic subpolar gyre

G. Koman [a,*], W.E. Johns [a], A. Houk [a], L. Houpert [b], F. Li [c]

[a] Rosenstiel School of Marine and Atmospheric Science, University of Miami, Miami, FL, USA
[b] National Oceanography Centre, Southampton, United Kingdom
[c] Xiamen University, Xiamen, Fujian, China

A B S T R A C T

This study describes new transport estimates of the North Atlantic Current in the Iceland Basin, and uses these results along with other contemporaneous measurements to determine mass and overturning budgets for the eastern North Atlantic subpolar gyre. As part of the Overturning in the Subpolar North Atlantic Program (OSNAP), estimates of the North Atlantic Current are determined using three full-depth dynamic height moorings spanning the Iceland Basin and are supplemented by Argo and satellite altimetry data. Along with historical estimates of the exchanges over the Iceland-Scotland Ridge, additional OSNAP results from the Rockall Trough and Rockall-Hatton Bank regions are used to calculate transport budgets in different density layers over a broad portion of the eastern subpolar gyre. Results show that 13–14 Sv of the North Atlantic Current ($\sigma_\theta < 27.8$ kg m^{-3}) flow northward into the middle of the Iceland Basin through a primary baroclinic flow near 23.5°W and a secondary quasi-barotropic flow near 26°W. Together with the observed northward flow in the Rockall-Hatton area, we conclude that 19–20 Sv of the upper limb of the Atlantic Meridional Overturning Circulation ($\sigma_\theta < 27.56$ kg m^{-3}) flows into the region where nearly 40 % of it (7.3 Sv) is converted into the lower limb primarily through progressive water mass modification from atmospheric cooling. This accounts for nearly half of the strength of Atlantic Meridional Overturning Circulation defined by the full OSNAP array extending across the basin from Greenland to Scotland.

1. Introduction

The Atlantic Meridional Overturning Circulation (AMOC) is a fundamental component of Earth's climate system. Warm, salty waters from the North Atlantic Current propagate to the subpolar and polar regions of the northern North Atlantic and Norwegian Sea where they experience buoyancy loss through cooling then return southward as North Atlantic Deep Water. Despite its importance, continuous trans-basin monitoring of this process did not begin until 2014 with the advent of the Overturning in the Subpolar North Atlantic Program (OSNAP; Lozier et al., 2017). This program now maintains the first continuous Eulerian array across the entire northern North Atlantic to improve our knowledge of the subpolar gyre's fluxes of heat, mass and freshwater (Fig. 1). Prior to OSNAP it was believed that the formation of deep waters within the lower limb of the AMOC occurred primarily in two locations: through dense overflows from the Norwegian Seas and deep convection in the Labrador Sea. However, one of the first papers produced from the OSNAP program found that there was very little overturning in the Labrador Sea, leaving the location of much of the overturning undocumented (Lozier et al., 2019).

In order to gain a better understanding of the AMOC, accurate estimates of the transport in its upper and lower limbs within the North Atlantic subpolar gyre, and the rates and locations of water mass conversion between them, are necessary. This study aims to update the geostrophic transport of the North Atlantic Current flowing into the Iceland Basin using a combination of OSNAP moorings, autonomous Argo floats, and satellite altimetry. Then, combined with other recent results from the OSNAP program, this study establishes a mass balance and evaluates overturning in the eastern North Atlantic subpolar gyre. The boundaries of the study domain are defined by the Reykjanes Ridge in the west, the European continent in the east, the OSNAP line near 58°N in the south, and the Iceland-Scotland Ridge in the north (Fig. 1). The flow across each of the oceanic boundaries of this domain is divided into three potential density layers, using two isopycnals to separate the water masses. The chosen isopycnals are $\sigma_\theta = 27.56$ kg m^{-3}, which is the potential density of the maximum in the overturning streamfunction (i.e., the isopycnal at which the maximum of the overturning streamfunction in density space occurs) along the OSNAP mooring line between Greenland and Scotland (Li et al., 2021), and $\sigma_\theta = 27.8$ kg m^{-3}, which is the isopycnal separating cooler recirculating subpolar gyre water from the denser waters that originate from the Nordic Sea overflows. Waters in the upper layer therefore constitute the upper limb of the AMOC ($\sigma_\theta < 27.56$ kg m^{-3}), while the combined flow in the bottom two layers constitute the lower limb ($\sigma_\theta > 27.56$ kg m^{-3}).

* Corresponding author.
E-mail address: gregory.koman@whoi.edu (G. Koman).

https://doi.org/10.1016/j.pocean.2022.102884
Received 20 August 2021; Received in revised form 6 April 2022; Accepted 1 September 2022
Available online 6 September 2022

2. Background

In the following, we describe the available historical measurements and recent estimates from OSNAP of the flow across each of the main boundaries in the eastern North Atlantic subpolar gyre east of the Reykjanes Ridge and between the OSNAP line near 58°N and the Iceland-Scotland Ridge. This provides a baseline of estimates in the region that we later update based on new results (Section 4.1) and adjust for the purposes of attaining a mass balance (Section 4.2). The order of the descriptions follows the general path of the gyre (Fig. 1), beginning with the North Atlantic Current entering from the south through the Iceland Basin, over the Rockall Plateau and through the Rockall Trough (Sections 2.1–2.3). We then discuss the exchanges over the Iceland-Scotland Ridge (Section 2.4), the outflows over the Reykjanes Ridge in the west (Section 2.5), and the flows exiting the Iceland Basin via the East Reykjanes Ridge Current and Iceland Scotland Overflow Water in the southwest (section 2.6).

2.1. Iceland Basin and the North Atlantic Current

Within the central and eastern Iceland Basin, the circulation is mostly distinguished by the warmer waters of the North Atlantic Current entering from the south. These waters, along with the northward flow over the Rockall Plateau and through the Rockall Trough to the east, are recognized as the primary conduits of the upper AMOC in the North Atlantic subpolar gyre. Previous studies of the North Atlantic Current in the Iceland Basin found that it is broad and highly variable with speeds of 2–30 cm s^{-1} over a section hundreds of kilometers wide (Bower et al., 2002; Rossby et al., 2000; van Aken & Becker, 1996; Knutsen et al., 2005; Fratantoni, 2001). As an extension of the Gulf Stream, much of this flow constitutes some of the warmest and saltiest (>35.1 psu) waters in the North Atlantic subpolar gyre (Sarafanov et al., 2012; Daniault et al., 2016). Transport estimates in the Iceland Basin are complicated by significant eddy activity in the region, with many of the eddies being viewed as quasi-stationary (Shoosmith et al., 2005; Read & Pollard, 2001; Wade & Heywood, 2001; Chafik et al., 2014; Zhao et al., 2018; Heywood et al., 1994). This eddy activity extends through much of the region, including from the Hatton Bank to all parts of the interior basin deeper than 2000 m. While many schematics show idealized representations of the North Atlantic Current entering the basin, the broadness of the flow combined with the eddy activity suggests that it is a much more complicated phenomenon.

As a result of this broad, meandering flow, previous estimates of the transport of the North Atlantic Current into the Iceland Basin have varied. Several studies in the 1990s found that this transport was about 20–25 Sv (Bacon, 1997; Sy et al., 1992; van Aken & Becker, 1996; Krauss, 1995). More recently, a publication from Lozier et al. (2019) suggests that the upper AMOC transport (σ_θ < 27.66 kg m^{-3}) in the interior Iceland Basin is slightly <10 Sv, with an additional ~6 Sv of northward transport along the Hatton Bank slope. Other recent studies (Daniault et al., 2016; Mercier et al., 2015; Sarafanov et al., 2012) estimate that 16–20 Sv of the upper AMOC (σ_1 < 32.15) flows into the Rockall Trough and Iceland Basin, with ~90 % of the transport flowing into the latter (Bower et al., 2019). These studies, along with other analyses farther upstream near the Mid-Atlantic Ridge, found full top-to-bottom estimates of the North Atlantic Current varying from 27 Sv to 50 Sv (Paillet & Mercier, 1997; Roessler et al., 2015; Daniault et al., 2016) depending on the geographical constraints and definitions of the transport. In this study we provide a new 4-year mean estimate of the North Atlantic Current in the Iceland Basin to compare with previous results and to aid in the construction of mass and overturning budgets.

2.2. Rockall Plateau

The Rockall Plateau, also known as the Rockall-Hatton Plateau, is a ~500 km wide portion of shallow topography in the northeast North Atlantic situated between the Iceland Basin to the west and the Rockall Trough to the east. The main features of the Plateau include the Hatton Bank to the northwest and the Rockall Bank to the southeast, with the Rockall-Hatton Basin in the middle separating the two features (Fig. 1). Most available North Atlantic Current transport estimates combine the flows in this region with those in the Iceland Basin to produce one total estimate. In many cases, this bulk transport value includes portions of the North Atlantic Current flowing into the Rockall Trough to the east as well (Daniault et al., 2016; Mercier et al., 2015; Sarafanov et al., 2012).

As part of the OSNAP program Houpert et al. (2018) presented a detailed analysis of the mean transport over the Rockall Plateau from 16 glider sections between June 2014 and June 2016. Their study separated

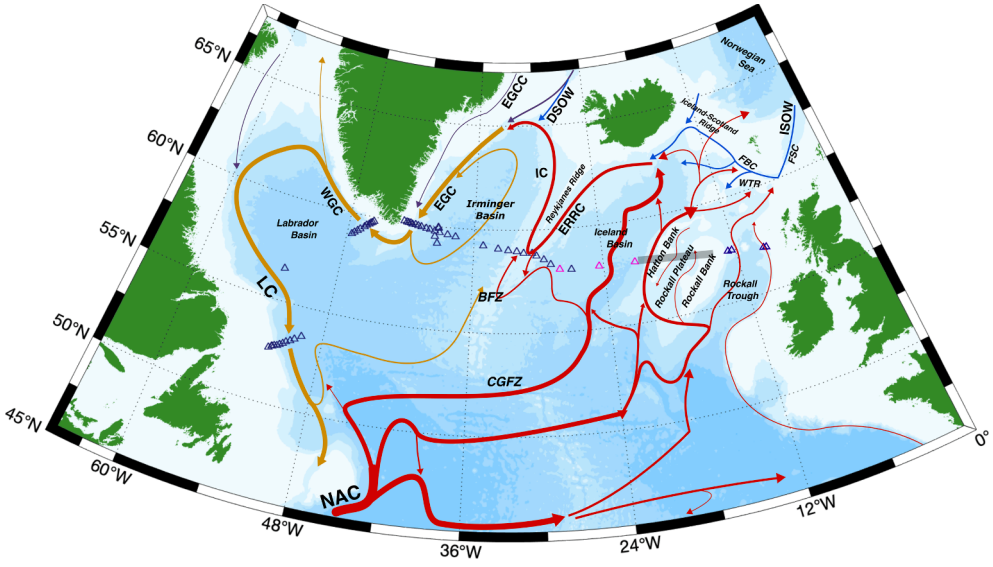

Fig. 1. Schematic of the surface water pathways (red, yellow and green) and deep water pathways (blue) in the North Atlantic subpolar gyre, adapted from Koman et al. (2020). Green and red arrows depict surface waters primarily of Arctic origin and North Atlantic Current origin while yellow arrows represent surface waters with mixtures of both. All mooring locations in the OSNAP program are denoted by triangles with the moorings used in this study to determine the transport of the North Atlantic Current in the Iceland Basin in magenta. The location of the OSNAP glider section is pictured in gray over the Rockall Plateau in line with the moorings in the Iceland Basin and Rockall Trough. Bathymetry colors change with every 1000 m in depth. Acronyms: East Reykjanes Ridge Current (ERRC); Irminger Current (IC); Denmark Strait Overflow Water (DSOW); East Greenland Coastal Current (EGCC); East Greenland Currents (EGC); West Greenland Current (WGC); Labrador Current (LC); North Atlantic Current (NAC); Iceland Scotland Overflow Water (ISOW); Faroe Shetland Channel (FSC); Faroe Bank Channel (FBC); Wyville Thomson Ridge (WTR); Charlie Gibbs Fracture Zone (CGFZ); Bight Fracture Zone (BFZ). (For interpretation of the references to color in this figure legend, the reader is referred to the web version of this article.)

the transport into two northward flowing jets along the western slopes of the Hatton Bank and the Rockall Bank (the Hatton Bank Jet and the Rockall Bank Jet, respectively), and another topographically constrained southward recirculation feature between the two jets over the eastern slope of the Hatton Bank. The two features in the east were found to have relatively weak transports that tended to compensate for each other (1.5 ± 0.2 Sv for the Rockall Bank Jet and −1.5 ± 0.4 Sv for the southward recirculation), while the Hatton Bank Jet was responsible for 5.1 ± 0.9 Sv of transport into the Iceland Basin. However, the Hatton Bank transport estimate used in this study includes a westward extension that aligns with the eastern edge of the North Atlantic Current region examined in this study; this reduces the Hatton Bank transport estimate to 4.5 Sv due to the inclusion of a southward recirculation (as discussed in Section 4.1). This amount is similar to the total inferred from the study by Lozier et al. (2019) of ~4 Sv. Although the results from Houpert et al. (2018) are synoptic glider sections instead of continuous time-series estimates, they provide the most detailed observations collected to date across this region.

2.3. Rockall Trough

The warmest and most saline waters of the North Atlantic subpolar gyre are found in the surface waters of the Rockall Trough. Here the middle branch of the North Atlantic Current (Fig. 1) propagates waters of subtropical origin into the gyre as part of the upper limb of the AMOC. These waters flow into the basin at two primary locations: a smaller buoyancy-driven current in the east confined to the flank of the continental shelf at depths < 1000 m, and a larger flow in the basin's interior (Houpert et al., 2020). Studies from the Extended Ellett Line program (Holliday et al., 2000; Holliday et al., 2015) found a net northward transport of 3–4 Sv of the upper AMOC through the Rockall Trough using a mid-depth level of no motion. More recently, results from the first continuous observations in the Rockall Trough from OSNAP have found stronger net transports of 5.2 Sv (Lozier et al., 2019) from 21 months of data (2014–2016) and 4.5 ± 0.8 Sv (Houpert et al., 2020) from 4 years of data (2014–2018). The latter study also found notable seasonality with an increased transport of 6.3 Sv in October followed by a rapid spin-down to 2.8 Sv in January associated with a diversion of the North Atlantic Current from the Rockall Trough entrance to the west of the Rockall Bank. This study will use the 4.5 ± 0.8 Sv value from Houpert et al. (2020) for the best estimate of transport through the Rockall Trough because it is derived from the longest continuous time series in the basin.

2.4. Iceland-Scotland Ridge

The Iceland-Scotland Ridge has been a location of great interest and detailed study for decades. Here the warm, salty waters from the North Atlantic Current flow northward over the ridge to the Norwegian Sea where they cool and sink. Much of this water then overflows back across the ridge in the form of Norwegian Sea Deep Water and Norwegian Sea Arctic Intermediate Water (Beaird et al., 2013). This diapycnal water transformation plays a critical role in the AMOC because this process creates the source waters for lower North Atlantic Deep Water.

The Faroe Islands divide the Iceland-Scotland Ridge into two sections, with the longer portion to the west between the Faroe Islands and Iceland. Significant temporal and spatial variations in transport over this broad section of the ridge, along with vulnerabilities to oceanographic equipment due to frequent fishing operations, have made long term studies of exchanges in this region challenging (Østerhus et al., 2019; Perkins et al., 1998; Rossby et al., 2009; Rossby et al., 2018). However, the Atlantic-origin waters that move northward across the ridge quickly condense into a narrow eastward-flowing boundary current along the northern slope of the Faroe Islands which presents a more accessible location to monitor. Here, regular hydrographic surveys and moored Acoustic Doppler Current Profilers (ADCPs) have been deployed since the late 1980s and a recent analysis has combined this data with altimetry to create a robust multi-decadal time series (Hansen et al., 2015). From this analysis, Hansen et al. (2015) inferred a mean transport of 3.8 ± 0.5 Sv of Atlantic waters across the ridge defined by a combination of the 4 °C isotherm and the 35.00 psu isohaline. We will use this transport value for our estimate of flow into the Norwegian Sea between Iceland and the Faroe Islands.

Despite the perennial interest in the exchanges over the Iceland-Scotland Ridge, finding a consistent transport estimate of the deep overflow waters between Iceland and the Faroe Islands has been elusive due to the intermittent nature of this flow and the large spatial scale of the ridge (>300 km). Several analyses have concluded that ~1 Sv of overflow water crosses the ridge southward into the Iceland Basin, though none of these estimates use continuous time-series observations along the entire ridge (Beaird et al., 2013; Perkins et al., 1998; Hermann, 1967). Instead, studies have mostly focused on two locations near the two ends of the ridge where most of the overflow is believed to cross (Rossby et al., 2009; Hansen et al., 2018). The location in the west near Iceland – known as the Western Valley – has historically been thought to carry the strongest transport (Perkins et al., 1998; Voet, 2010; Olsen et al., 2016), although recent direct measurements there using a moored ADCP and two bottom temperature loggers found only 0.02 ± 0.05 Sv over a 278 day period (Hansen et al., 2018). The other location of focus, at the deepest part of the ridge crest near the Faroe Islands, contributes intermittently to the overflow (Østerhus et al., 2008; Beaird et al., 2013) and a three-year glider survey from Beaird et al. (2013) found a transport of 0.3 ± 0.3 Sv through this part of the ridge. Therefore, these newest observations led Østerhus et al. (2019) to conclude that the total overflow transport between Iceland and the Faroe Islands is only 0.4 ± 0.3 Sv, and we will use this value as our estimate of the overflow transport across the Iceland-Faroes Ridge.

To the east of the Faroe Islands additional North Atlantic Current water flows northward into the Norwegian Sea while Norwegian overflow waters pass southward beneath it through the Faroe Shetland Channel. Over the past few decades, studies of the surface-intensified North Atlantic water have found approximately 3–4 Sv of northward transport in this region (Turrell et al., 1999; Hughes et al., 2006; Sherwin et al., 2008). However, many of these values were from short-term or synoptic studies. More recently, Berx et al. (2013) used *in situ* and long-term altimetry observations (1993–2011) to conclude that the transport was slightly lower (2.7 ± 0.5 Sv). Østerhus et al. (2019) extended the analysis by a few more years (through 2015) and found the same estimate, so we will use this value for our transport of North Atlantic Current waters into the Norwegian Sea between the Faroe Islands and the European continent.

Most of the overflow waters passing through the Faroe Shetland Channel continue to the Faroe Bank Channel where they enter westward into the deep Iceland Basin. The most comprehensive study of the Faroe Bank Channel overflow is from Hansen et al. (2016), who found 2.2 ± 0.2 Sv of overflow water transport from nearly-two decades (November 1995 to May 2015) of continuous moored ADCP measurements. Additional overflow water from the Faroe Shetland Channel has been found to intermittently flow across the Wyville Thomson Ridge just upstream of the Faroe Bank Channel (Sherwin et al., 2008; Johnson et al., 2017). Previous studies at this location have reported transports ranging from 0.1 to 0.3 Sv (Hansen & Østerhus, 2000; Sherwin et al., 2008), with the most recent estimate finding 0.2 ± 0.1 Sv from over 5 years of monthly averages (Østerhus et al., 2019). Together with the overflow through Faroe Bank Channel, this yields a value of 2.4 ± 0.2 Sv for the overflow from the Faroe Shetland Channel that passes into the Iceland and Rockall Basins.

2.5. Reykjanes Ridge

The Reykjanes Ridge bounds the Iceland Basin on the west and is the approximate dividing line between the southward flowing East

Reykjanes Ridge Current in the western Iceland Basin and the northward flowing Irminger Current in the Irminger Basin. As part of the cyclonic flow around the North Atlantic subpolar gyre, waters from the East Reykjanes Ridge Current flow across the Reykjanes Ridge to partly feed the Irminger Current. The region along the Reykjanes Ridge crest to the north of the OSNAP line (near 59°N) is one of the least studied sections discussed in this paper. Volume conserving box models (Treguier et al., 2005; Lherminier et al., 2010; Sarafanov et al., 2012) have estimated transports across the ridge in the range of 9–15 Sv, while a study of shipboard ADCP data repeatedly crossing over the Reykjanes Ridge (Chafik et al., 2014) has suggested that the transport is minimal. Petit et al. (2019) reported the first direct estimates of transport over the ridge at these latitudes from hydrographic stations referenced to shipboard ADCP data, finding a westward geostrophic transport north of the OSNAP line of 13.8 ± 0.7 Sv. Koman et al. (2020) used the Roemmich-Gilson Argo climatology (Roemmich & Gilson, 2009) referenced to absolute mean sea level from multi-mission satellite altimeter data to estimate the longer-term mean flow across the ridge for the period from 2004 to 2016. They found a weaker transport over the ridge (6.8 ± 2.2 Sv) upstream of the OSNAP line, with most of it occurring within 100 km of the line as the East Reykjanes Ridge Current begins to turn westward into the Irminger Basin.

Each of these observational estimates have their shortcomings. While Petit et al.'s (2019) transport estimate is highly accurate, it is from a single synoptic study in a region of high temporal variability (Sarafanov et al., 2012, Koman et al., 2020). The estimates from Koman et al. (2020) are a time-mean calculation but using altimetry as a reference velocity may not fully resolve finer mesoscale features near topography, potentially resulting in an underestimate of velocity (Chafik et al., 2014; Pujol et al., 2016; Houpert et al., 2020; Koman et al., 2020). Koman et al. (2020) also analyzed three OSNAP cruise sections along the Reykjanes Ridge and found that those synoptic realizations of the flow over the ridge varied widely (their Fig. 10). This suggests that, despite the shortcomings of altimetry, a mean transport is likely to be the best estimate. Therefore, the transport budget in this study will use the 6.8 ± 2.2 Sv value from Koman et al. (2020), with the caveat that biases in the altimetry data could possibly lead to an underestimate of the true transport.

2.6. East Reykjanes ridge current and Iceland Scotland overflow water

Two currents flow southward along the eastern flank of the Reykjanes Ridge: the East Reykjanes Ridge Current and the Deep Western Boundary Current carrying dense waters from the Iceland Scotland Overflow plume. The East Reykjanes Ridge Current is a nearly barotropic flow trapped close to the crest of the Reykjanes Ridge while the Iceland Scotland overflow plume is a bottom-intensified flow extending from the upper RR slope to the edge of the deep Iceland Basin (Koman et al., 2020; Johns et al, 2021).

The surface waters of the East Reykjanes Ridge Current consist of Subpolar Mode Water formed from the recirculation of the portion of the North Atlantic Current that remains in the Iceland Basin instead of crossing the Iceland-Scotland Ridge (Brambilla & Talley, 2008; Koman et al., 2020). The deepest waters of the quasi-barotropic East Reykjanes Ridge Current originate from modified Iceland Scotland Overflow water - commonly referred to as Icelandic Slope Water - that forms along the Iceland-Scotland Ridge (Koman et al., 2020; Beaird et al., 2013). At intermediate depths, modified Labrador Sea Water mixes into the East Reykjanes Ridge Current which creates a salinity minimum at a potential temperature near 3.7–4.0 °C at a depth of ~1400 m (Koman et al., 2020). Estimates of the transport of the East Reykjanes Ridge Current have only recently been established, and in fact this current was first named in 2005 (Treguier et al., 2005).

Some of the first estimates of the East Reykjanes Ridge Current's transport came from the Observatory of Interannual and Decadal Variability in the North Atlantic project (OVIDE) which found a mean transport of 8.9 Sv for water above the $\sigma_\theta = 27.8$ isopycnal from repeat hydrographic sections near 59°N (Daniault et al., 2016). At this same location, Petit et al. (2019) found a transport of 10.6 Sv from a synoptic hydrographic study in the summer of 2015. The most recent estimate (Koman et al., 2020) found a time-mean transport of 11.7 ± 0.5 Sv from a 4-year mooring time series from the OSNAP program using current meters, temperature-salinity sensors and ADCPs. Given that the East Reykjanes Ridge Current has high temporal variability (Koman et al., 2020), the continuous multiyear transport calculation from Koman et al. (2020) will be considered the best estimate of this flow and used in the transport budget in this study.

Norwegian Sea Deep Water flows into the Iceland Basin primarily through the Faroe Bank Channel with additional contributions over the sill between Iceland and the Faroe Islands (Beaird et al., 2013). These are the headwaters of North Atlantic Deep Water and a conduit of the lower limb of the AMOC. Previous studies have found that this water descends at a rate of ~3 Sv into the Iceland Basin (Saunders, 1996; Hansen & Østerhus, 2007; Olson et al., 2008) where it may experience a < 1 Sv increase in transport from entrainment as it becomes Iceland Scotland Overflow Water (Saunders, 1996; Kanzow & Zenk, 2014). Iceland Scotland Overflow Water then moves southward in the western Iceland Basin (Hansen & Østerhus, 2000; Beaird et al., 2013; Harvey & Theodorou 1986; Saunders 1996; Fogelqvist et al. 2003) beneath the East Reykjanes Ridge Current before mostly exiting at the Charlie Gibbs Fracture Zone, where estimates have found ~2 Sv crossing into the Irminger Basin (Bower & Furey, 2017; Saunders, 1994; Xu et al., 2010). Some additional leakage of Iceland Scotland Overflow Water through other Reykjanes Ridge fracture zones farther upstream also appears to take place (Quadfasel & Käse, 2007; Saunders, 1994; Xu et al., 2010; Bower & Furey, 2017). However, a recent study (Johns et al., 2021) has found a substantially larger southward transport of Iceland Scotland Overflow Water in the Iceland Basin (5.3 ± 0.4 Sv) based on a 4-year record from moored current meters and temperature/salinity recorders as part of the OSNAP program. Given that this is the longest continuous time series of Iceland Scotland Overflow Water on record, and that it is measured directly at the site of this study, our transport budget will use this value as the most updated estimate of Iceland Scotland Overflow Water transport at the OSNAP line.

3. Data and methods

3.1. OSNAP moorings in the Iceland Basin

The OSNAP array extends from Canada across the Labrador Basin to Greenland, and from Greenland across the Irminger and Iceland basins to Scotland (Fig. 1). The array in the Iceland Basin is arranged to capture the broad inflow from the North Atlantic Current (Fig. 2). The U.S.-supported (University of Miami) array in this area consists of dynamic height moorings M2, M3 and M4 that provide spatially-integrated geostrophic estimates of the North Atlantic Current flowing into the region. Temperature and salinity (T/S) recorders, current meters and upward-looking ADCPs on these moorings have provided continuous data in three separate deployments for the period from July 2014 to July 2018.

To derive estimates of the North Atlantic Current's transport and vertical structure, the OSNAP data is initially passed through a 40-hour low pass filter to remove sub-inertial variability associated with internal/inertial waves and tides. Shape-preserving splines are then used to interpolate between T/S recorders to give full depth property profiles at the moorings to within 50 m of the surface (the shallowest measurement level of each mooring). To extend these profiles to the surface, the 50 m temperature readings are compared to 1/20th degree satellite-derived sea surface temperature data from the Group for High Resolution Sea Surface Temperature (GHRSST) that is interpolated to the location of the mooring site. This data is produced by the Jet Propulsion Laboratory and obtained through the Asia-Pacific Data Research Center. If GHRSST is

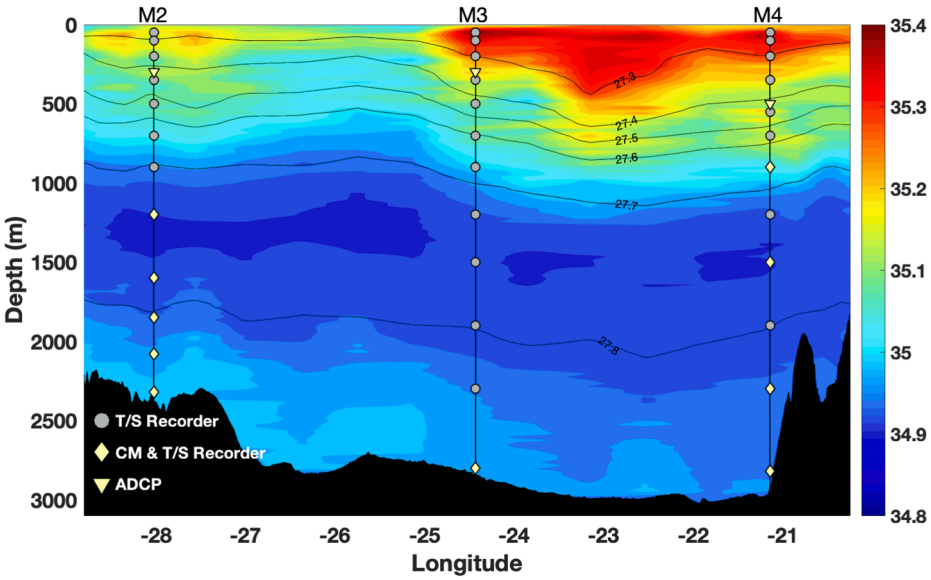

Fig. 2. Southern view of the OSNAP moorings used in this study in the Iceland Basin near 58°N. Colored contours show salinity (psu) from a section of CTD stations from the summer of 2016; black contour lines are sigma-theta surfaces (kg m^{-3}). Moored instruments are designated by circles (temperature-salinity recorders), diamonds (current meters and temperature-salinity recorders), and upside-down triangles (upward-looking Acoustic Doppler Current Profilers).

warmer than the 50 m temperature, GHRSST is used as the surface temperature point in the vertical spline interpolation; otherwise the 50 m temperatures are extended to the surface. The latter scenario only occurs when a deep mixed layer is present but yields much more accurate results based on an analysis comparing Argo surface temperatures to 50 m Argo temperatures and GHRSST. Lacking any more accurate estimate of surface salinity, measured salinity values at 50 m were duplicated to the surface. Using these full depth T/S profiles, the horizontally averaged geostrophic velocity profile is calculated between the moorings and expressed as a transport-*per*-unit-depth profile between them. These profiles are then integrated upwards from the $\sigma_\theta = 27.8$ kg m^{-3} isopycnal to give the baroclinic geostrophic transport relative to the surface. Transport below 27.8 kg m^{-3} is considered to be Iceland Scotland Overflow Water (Dickson & Brown, 1994; Saunders, 1996) and is not included in our derived transport estimates for the North Atlantic Current. The relative geostrophic transport is then referenced to the horizontally averaged surface velocity measured from altimetry between the moorings to create an absolute estimate of the transport-*per*-unit-depth profile and to calculate the total transport between moorings.

3.2. CMEMS all-satellite altimetry

The Copernicus Marine Environmental Monitoring Service (CMEMS) absolute sea level product comes from multi-mission altimeter satellites and is processed to a ¼ degree gridded sea surface height computed with respect to its twenty-year mean since 1992. The absolute dynamic topography derived from this product is used to calculate surface reference velocities between moorings M2, M3 and M4 to produce an estimate of the absolute geostrophic transport between the moorings. This daily product is interpolated to hourly data as an integrated transport-*per*-unit-depth at the sea surface (m^2/s), which is then added to the baroclinic geostrophic transport profile between moorings. Vertical integration of this profile then leads to an altimetry-referenced estimate of absolute transport.

3.3. Argo data

Argo profile data is taken from the Roemmich-Gilson Argo climatology, which is produced and distributed by the Scripps Institution of Oceanography. This product contains temperature and salinity data at 58 different pressure levels and has global coverage of ⅙ degree resolution (Roemmich & Gilson, 2009). This product is based on data from 1998 to 2018 and is used to resolve the depth-dependent spatial distribution of velocities and mean water mass properties of the North Atlantic Current.

Argo displacement drift data, which is used to calculate velocities at the 1000 m parking level based on the displacement of Argo floats between diving cycles (Lebedev et al. 2007), is used as a reference velocity for the baroclinic shear created from the Roemmich-Gilson data. This data is also used as an alternative (time mean) reference velocity for the relative transports from the mooring data. This ¼ degree mean product includes data from 1997 to 2016 and is made available through the Asia-Pacific Data-Research Center (APDRC). The Argo-derived baroclinic shear is interpolated to ¼ degree and referenced to the 1000 m Argo drift displacement data to resolve Argo-based mean velocities throughout the upper 2000 m water column (Bilo & Johns, 2019; Bilo, 2019).

3.4. OSNAP analysis

An integrated analysis of all OSNAP observations across the full trans-basin array, as described in Li et al. (2017) and Lozier et al. (2019), is used in this paper to compare with the individual results from each section. In addition to the OSNAP data, this analysis incorporates available Argo and altimetry data, and applies an overall mass balance across the array to further constrain the flow. Details of this procedure, which we refer to hereafter to as the "OSNAP analysis," can be found in Li et al. (2017).

4. Results and discussion

4.1. North Atlantic Current in the Iceland Basin

The four-year time series of the North Atlantic Current transport between moorings M2 and M4 is displayed in Fig. 3a. The time series is calculated by determining the relative geostrophic transport from the three dynamic height moorings in the Iceland Basin (M2-M4) and referencing it to surface altimetry to determine the absolute geostrophic transport. This results in a mean transport of 13.2 ± 0.6 Sv with a standard deviation of 4.9 Sv. The Argo derived mean transport from 1000 m Argo drift data gives a similar transport value (14.0 ± 0.9 Sv).

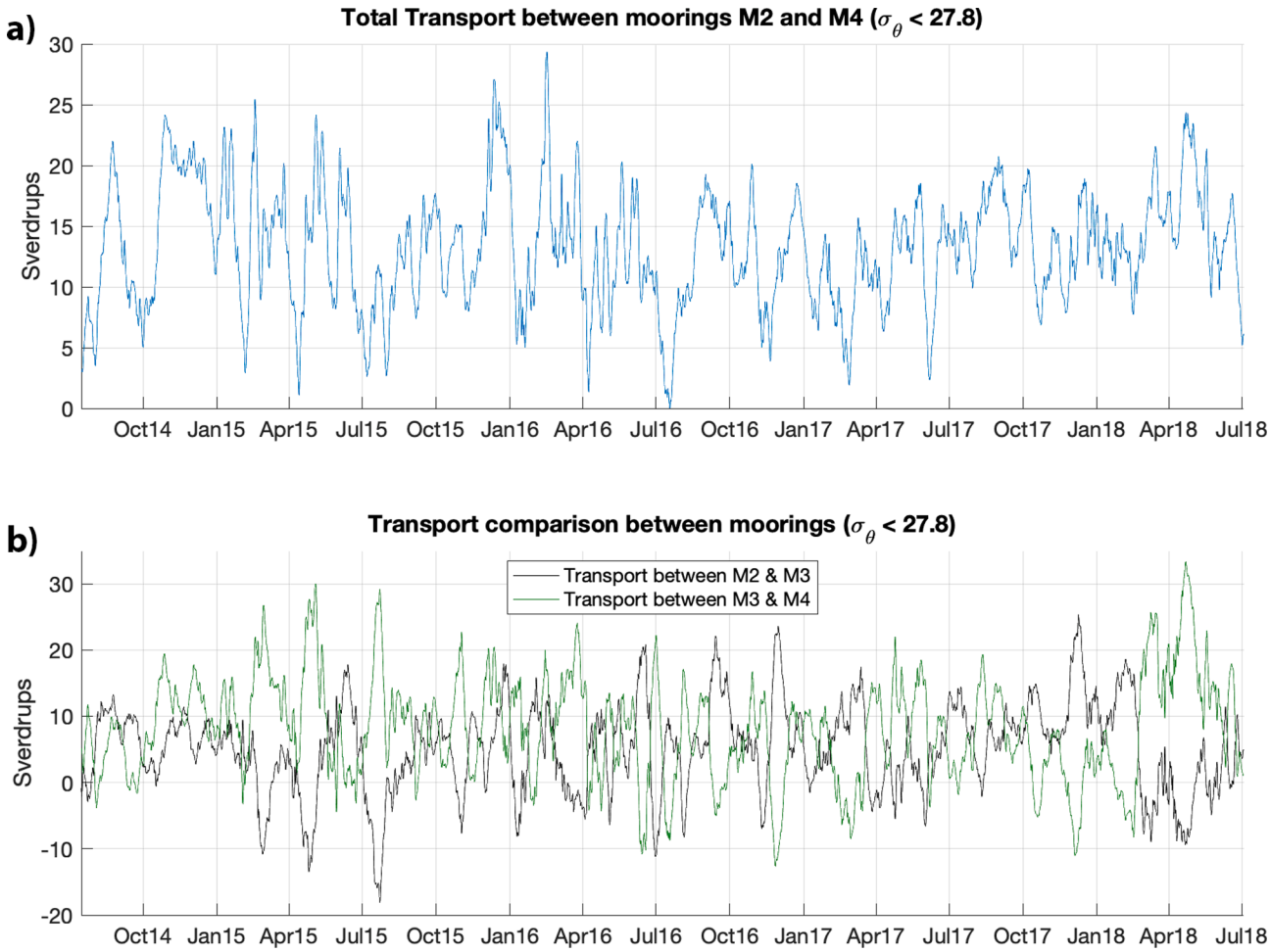

Fig. 3. 40-hour lowpass filtered transport time series of the North Atlantic Current ($\sigma_\theta < 27.8$ kg m^{-3}) in the Iceland Basin from 4 years of OSNAP data. Fig. 3a shows the total transport time series between moorings M2 and M4 using dynamic height moorings referenced to altimetry. Fig. 3b shows the altimetry-referenced transports separated by mooring sections (M2-M3 in black and M3-M4 in green). Positive values represent the prevailing direction of the North Atlantic Current to the north. Fig. 3a has a mean northward transport of 13.2 Sv, with a standard deviation of 4.9 Sv and a standard error of 0.6 Sv. Fig. 3b has a mean northward transport between moorings M2-M3 of 5.1 Sv, with a standard deviation of 6.7 Sv and a standard error of 0.9 Sv, while the mean transport between M3-M4 is 8.2 Sv, with a standard deviation of 7.8 Sv and a standard error of 1.2 Sv. (For interpretation of the references to color in this figure legend, the reader is referred to the web version of this article.)

Standard errors (henceforth the uncertainties associated with all transport means) for the altimetry-derived transports are calculated using an integral time scale of 11.7 days from the combined time series data and, for the Argo-derived transports, by summing the standard errors provided by the 1000 m gridded Argo drift data with the standard errors from the mooring data. The transport across the M2-M4 section that lies within the upper limb of the AMOC as defined by Lozier et al. (2019) (i.e., waters with $\sigma_\theta < 27.66$ kg m^{-3}) is 9.0 ± 0.8 Sv from altimetry reference and 9.2 ± 0.6 Sv from Argo reference, which matches well with Lozier et al.'s (2019) estimate of nearly 10 Sv.

The baroclinic transport of the North Atlantic Current derived from moorings M2-M4 (not shown) has a positive trend of 0.67 ± 0.30 Sv/year, though the overall North Atlantic Current transport after referencing by altimetry has a trend of only 0.06 ± 1.28 Sv/year. The trend in the baroclinic transport is significant (99 %) and indicates a steepening of the shear in the mean velocity profile over the 2014–2018 period. This is shown in Fig. 4a which displays the yearly mean velocity profiles between moorings M2 and M4 for each of the measurement years (averaged from summer to summer). The minimal trend seen in the total transport (Fig. 3a), despite the increasing baroclinic transport, can be explained by the strengthening of the surface velocity over time being countered by a general weakening of the flow at depth. The total transport ($\sigma_\theta < 27.8$ kg m^{-3}) decreases over the first three years (13.9 ± 1.3 Sv, 13.1 ± 1.1 Sv, 11.4 ± 0.9 Sv, respectively) before a strong increase in surface intensified flow results in a stronger transport in the fourth year of observations (14.6 ± 0.8 Sv), yielding the slightly positive (but insignificant) overall trend.

The transport time series for the regions between moorings M2-M3 and M3-M4 individually (Fig. 3b) show a range of variability that is much more pronounced than the variability across the entire M2-M4 section. Here we can see that extreme transport events in one section are often offset by the other section and actually temper the variability in the overall transport (e.g. May 2015, August 2015, December 2017, etc.). This leads to both individual sections having higher standard deviations (6.7 Sv for M2-M3; 7.8 Sv for M3-M4) than the entire North Atlantic Current transport between M2 and M4 (4.9 Sv). These offsetting transports result in a strong negative correlation between the M2-M3 and M3-M4 sections (-0.78), which we believe is due to westward propagating eddies in the central Iceland Basin and/or zonal meandering of the North Atlantic Current across the M3 mooring, as described further below.

The mean velocity profiles between moorings M2 and M3 and moorings M3 and M4 illustrate the spatial differences between the two mooring sections (Fig. 4b). Both profiles are strongly sheared in the top 1000 m as the surface-intensified northward-flowing North Atlantic Current crosses the OSNAP line, with the more pronounced shear

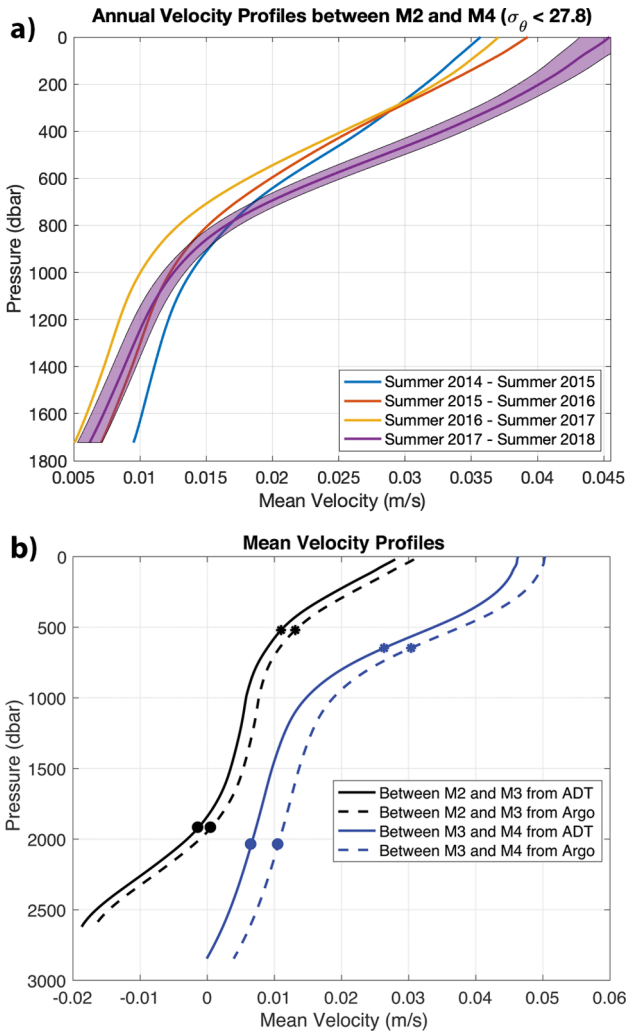

Fig. 4. (a) Yearly averaged (summer to summer) velocity profiles between M2 and M4 for the top 1700 m, and (b) four-year averaged full-depth profiles between moorings M2 and M3 and moorings M3 and M4), referenced to altimetry (solid lines) or Argo (dashed lines). Solid dots indicate the lightest isopycnal of Iceland Scotland Overflow Water (σ_θ = 27.8 kg m^{-3}) and asterisks mark the isopycnal of the maximum overturning in the streamfunction (σ_θ = 27.56 kg m^{-3}) along the OSNAP line east of Greenland. A standard error envelope is added to the 2017–2018 profile in (a) and is representative of the standard errors in the other profiles.

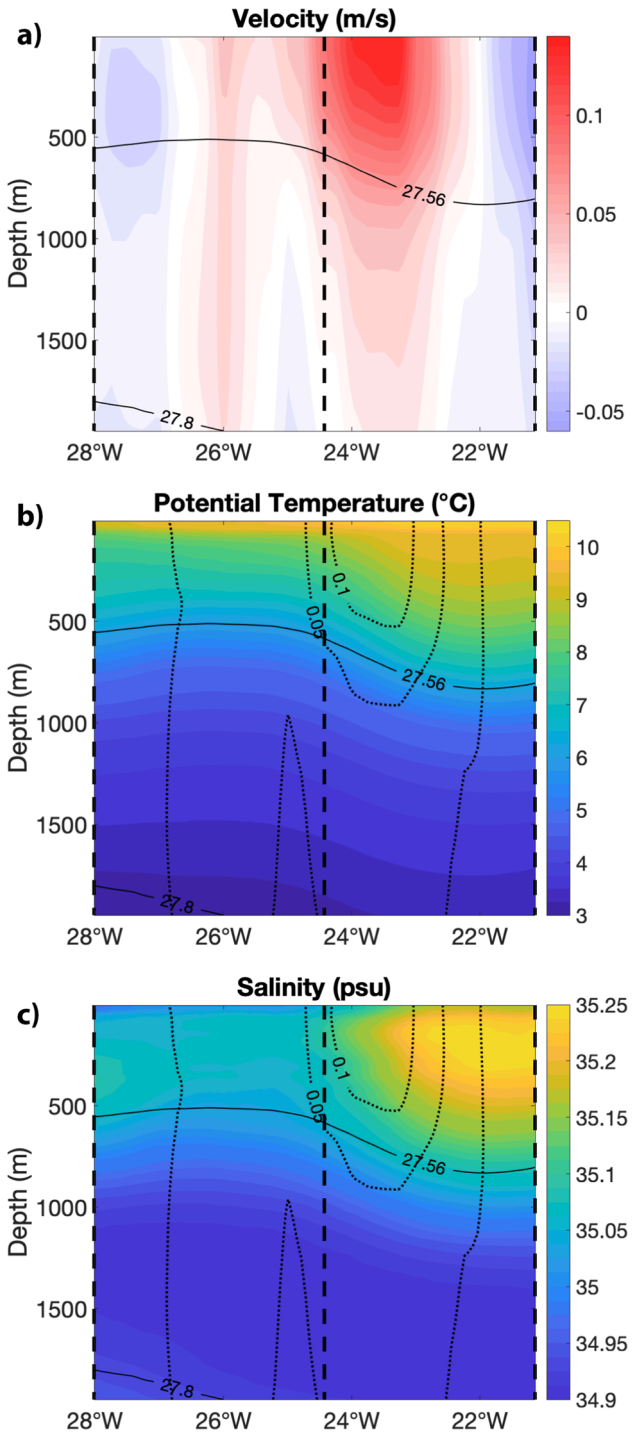

Fig. 5. Cross-sections of meridional velocity (a), potential temperature (b) and salinity (c) from mean Argo data between moorings M2, M3 and M4 from west to east. Moorings are marked by thick dashed vertical lines. Solid lines indicate the lightest isopycnal of Iceland Scotland Overflow Water (σ_θ = 27.8 kg m^{-3}) and the isopyncal of maximum overturning in the streamfunction (σ_θ = 27.56 kg m^{-3}) along the OSNAP line east of Greenland. Velocity contours are shown by dotted lines in 0.05 m s^{-1} increments (b, c).

located between moorings M3 and M4. At depth between moorings M2 and M3, the σ_θ = 27.8 kg m^{-3} isopycnal is located at a level of no motion separating the northward flowing waters of the North Atlantic Current from the southward flowing Iceland Scotland Overflow Water (Johns et al., 2021). Between M3 and M4 the northward flow extends to the bottom, which suggests that some of the Iceland Scotland Overflow Water recirculates northward back into the eastern part of the Iceland Basin. At mid-depth, we observe weak northward flow in both mooring sections.

Cross-sectional profiles from Argo (Fig. 5) give a more highly resolved view of the spatial structure of the time-mean velocity field across the M2-M4 domain, as well as the associated water mass properties. The velocity cross-section (Fig. 5a) shows a main branch of the North Atlantic Current entering the basin just to the east of mooring M3 near 23.5°W with an additional narrow branch near 26°W. According to Argo, the narrow branch has a more barotropic structure with mean velocities of 0.03–0.045 m s^{-1} extending through the entire 2000 m water column, while the main branch to the east is much more baroclinic with a maximum mean velocity of 0.14 m s^{-1} near the surface. Cross-sections of temperature (Fig. 5b) and salinity (Fig. 5c) reveal that the larger North Atlantic Current branch is saltier and warmer in the top 500 m, and marks the main front between the warm salty waters of subtropical origin to the east and the cooler fresher subpolar waters in the western part of the Iceland Basin. However, both the narrower western branch and the western part of the velocity core of the main

branch contain relatively fresh waters (<35.15 psu) that suggest an origin more from recirculated subpolar gyre water than subtropical waters from the Gulf Stream extension. Surface vector plots (not shown; see Koman et al., 2020; their Fig. 8) indicate that the narrow western branch recirculates westward into the East Reykjanes Ridge Current near 59°N while the majority of the main branch continues to the northern end of the Iceland Basin. This is consistent with general circulation patterns in the area from previous research (Bower et al., 2002). Koman et al. (2020) also show that some of the waters from both branches recirculate southward back across the OSNAP line at 58°N. This can be viewed at both ends of the velocity cross-section near mooring M2 in the west and mooring M4 in the east (Fig. 5a). The recirculation off the main branch near M4 is particularly strong and appears to be the result of a known quasi-stationary anticyclonic eddy (Martin et al., 1998) near 22°W with mean velocities greater than 0.05 m s^{-1}.

To evaluate the consistency between the two reference velocities used in this study, we compared their surface velocities by extending the 1000 m Argo drift data to the surface using the mean geostrophic shear from the Argo climatology (Fig. 6). These velocities compare remarkably well in intensity and spatial distribution given the differences in data sources. Both estimates show very little flow near mooring M2, but gradually increase to a maximum velocity of ~0.14–0.15 m s^{-1} as they reach the main branch of the North Atlantic Current to the east of M3. Both estimates also indicate the weaker secondary branch of the North Atlantic Current with a maximum velocity of >0.04 m s^{-1} to the west of mooring M3. The altimetry data suggests that this secondary flow is broader than seen in the Argo data, which could be due in part to spatial smoothing inherent in the gridded altimetry data. Finally, both velocities agree on a rapid reduction and then a reversal of velocity at the eastern end of the section in association with the quasi-permanent anticyclonic eddy centered just west of mooring M4.

A Hovmöller diagram of surface geostrophic velocities inferred from four years of altimetry data (Fig. 7) reveals the time-varying velocity changes across the M2-M4 mooring section. It shows clearly the persistent surface flow of the main branch of the North Atlantic Current to the east of mooring M3, which has some variability both spatially and in its intensity. While the velocities in the western branch are slower overall, they are more variable in strength and can often have speeds comparable to the main core. This appears to be the result of southward flow from westward propagating anomalies (e.g., eddies) splitting the main core and shifting much of it to the west of mooring M3. The Hovmöller plot reveals these westward propagating anomalies with some of them extending across nearly the entire section (e.g. August – December 2017). In some cases these anomalies are immediately preceeded or followed by velocities in the opposite direction, indicating eddies. In other cases, they appear to be meanders of part of the primary branch of the North Atlantic Current and are eventually followed by an eastward translation back to its original position (e.g. November 2017 – March 2018). These features can also be seen in the variations of transport between mooring sections (Fig. 3b). This passage of eddies and lateral shifts of the main NAC branch across mooring M3 explain the large negative correlation in transport observed between the M2-M3 and M3-M4 mooring sections seen in Fig. 3b.

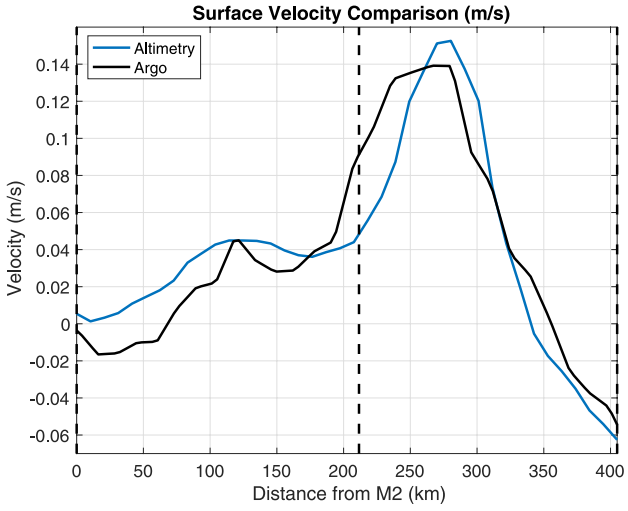

Fig. 6. Mean surface velocities from Argo (black) and altimetry (blue) between moorings M2, M3 and M4 from west to east. Mooring locations are marked by dashed vertical lines and distances are referenced to mooring M2. (For interpretation of the references to color in this figure legend, the reader is referred to the web version of this article.)

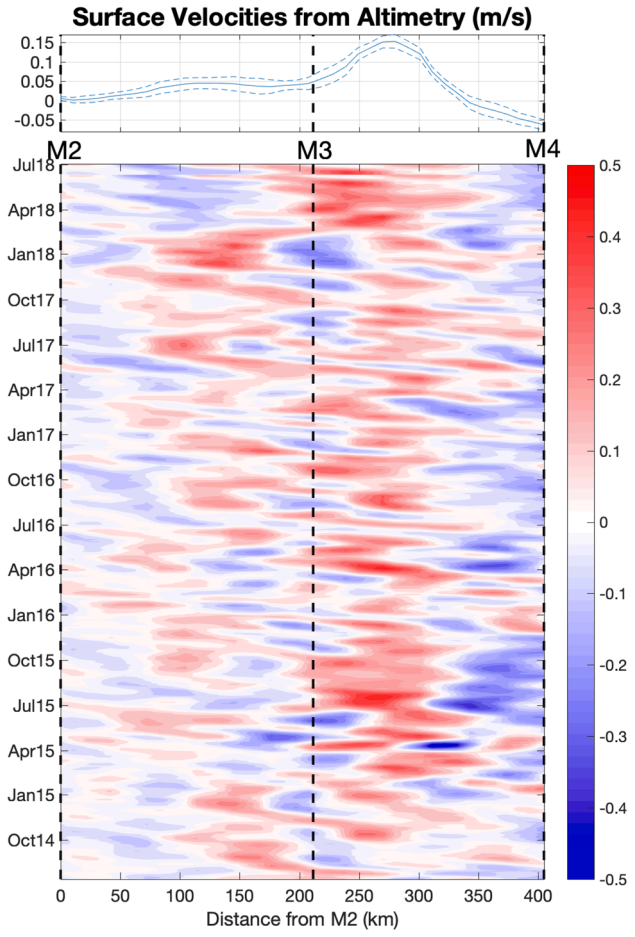

Fig. 7. Hovmöller diagram (bottom) of surface velocities (m/s) from altimetry between OSNAP moorings M2, M3 and M4 over a four-year period (July 2014 - July 2018), with mooring locations denoted by vertical black dashed lines. Positive values are in the prevailing direction of the North Atlantic Current to the north and distances are referenced to mooring M2. Four year mean velocities from altimetry as seen in Fig. 6 are indicated with standard errors (top).

4.2. *Eastern subpolar gyre mass and overturning budgets*

With these new estimates of the North Atlantic Current, we can construct a mass budget for the portion of the subpolar gyre between the Reykjanes Ridge in the west, the European continent in the east, the OSNAP line in the south, and the Iceland-Scotland Ridge in the north (Fig. 8). This budget is constructed from the transports across the bounding oceanic sections according to the results of this study and the related OSNAP and historical studies described in Section 2 (Table 1). To put our estimates in the context of overturning changes in the region, we divide the transports across each of these sections into three density

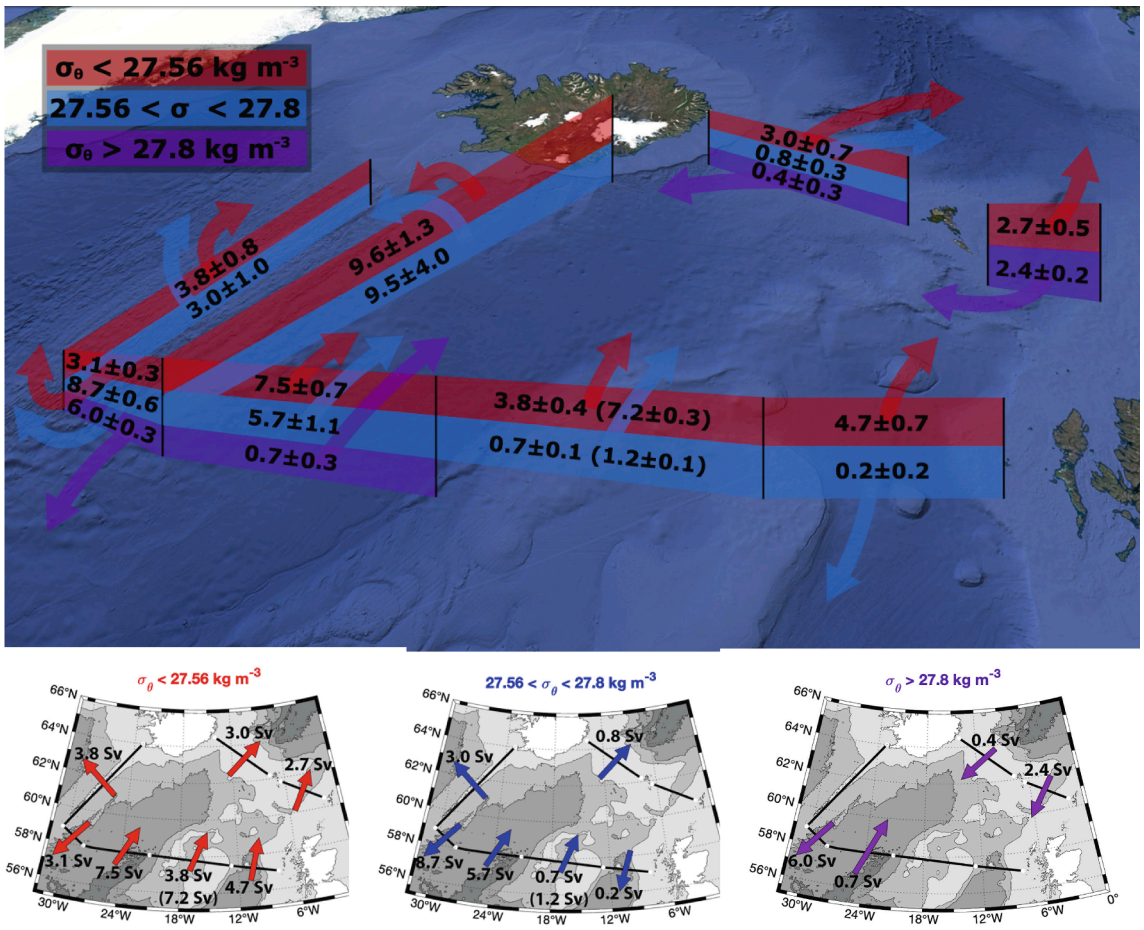

Fig. 8. Schematic of transport estimates (±std. error) by density layers determined by recent studies in the eastern North Atlantic subpolar gyre along the OSNAP line in the south, the Reykjanes Ridge in the west, and the Iceland-Scotland Ridge in the north. An additional section to evaluate the transport in the top two density layers through the middle of the Iceland Basin from Argo climatology is included. Estimates in parenthesis over the Rockall Plateau are from the OSNAP analysis. The three smaller bottom figures show the transports in each layer separately. All values in Sv. Schematic is meant for visual purposes and may not represent the exact geographical endpoints of each section, as described in Table 1.

Table 1
Transport estimates (±std. error) for the bounding sections of the region evaluated in this study, as displayed in Fig. 8. Positive transports are inflow into the region and negative values are outflow. Dashes indicate no transport in that layer for the given section. All values in Sv. Acronyms: North Atlantic Current (NAC); Iceland Scotland Overflow Water (ISOW); East Reykjanes Ridge Current (ERRC).

Transport Estimates	Upper Layer (σ_θ < 27.56 kg m^{-3})	Intermediate Layer (27.8 > σ_θ > 27.56)	Bottom Layer (σ_θ > 27.8 kg m^{-3})
Interior Iceland Basin NAC (21.1–28.0°W) and ISOW (21.1–24.4°W)	7.5 ± 0.7	5.7 ± 1.1	0.7 ± 0.3
Rockall Plateau (13.9–21.1°W) (Houpert et al., 2018)	3.8 ± 0.4	0.7 ± 0.1	–
Rockall Plateau (13.9–21.1°W) (OSNAP estimate)	7.2 ± 0.3	1.2 ± 0.1	–
Rockall Trough (8.8–13.9°W)	4.7 ± 0.7	−0.2 ± 0.2	–
Iceland-Scotland Ridge east of Faroe Islands (2.8–6.0°W)	−2.7 ± 0.5	–	2.4 ± 0.2
Iceland-Scotland Ridge west of Faroe Islands (7.9–13.7°W)	−3.0 ± 0.7	−0.8 ± 0.3	0.4 ± 0.3
Reykjanes Ridge (58.9–62.5°N)	−3.8 ± 0.8	−3.0 ± 1.0	–
ERRC (28.0–31.3°W) and ISOW (24.4–30.5°W)	−3.1 ± 0.3	−8.7 ± 0.6	−6.0 ± 0.3

layers separated by two isopycnals: σ_θ = 27.56 kg m^{-3}, which is the isopycnal of maximum overturning in the streamfunction along the OSNAP mooring line between Greenland and Scotland (Li et al., 2021), and σ_θ = 27.8 kg m^{-3}, which is the isopycnal separating intermediate subpolar gyre waters from the denser waters originating from the Norwegian Sea overflows. The upper density layer therefore contains waters that contribute to the net northward transport of the upper AMOC limb through the Greenland-Scotland OSNAP section, while the bottom two layers, in aggregate, carry the net southward transport of the AMOC's lower limb. In what follows, we describe the transports within each of these layers for the different sections and use the results to produce estimates of the diapycnal transport occurring between layers (i.e. overturning) within this broad northeastern subpolar domain.

First, the altimetry-referenced North Atlantic Current transport estimate found in this paper between moorings M2 and M4 of 13.2 Sv (σ_θ < 27.8 kg m^{-3}) – which we are using instead of the Argo-referenced transport due to the greater sample size of the altimetry data – is divided into the upper and intermediate layers. The same is done for the other inflow regions along the OSNAP line using data from recent studies over the Rockall Plateau (4.5 Sv; Houpert et al., 2018) and through the Rockall Trough (4.5 Sv; Houpert et al., 2020). The outflow over the Reykjanes Ridge (6.8 ± 1.3 Sv) and through the East Reykjanes

Ridge Current (11.7 ± 0.5 Sv) are separated into the upper and intermediate layers using the results from the recent study by Koman et al. (2020). Values of the transport in the Iceland Scotland Overflow Water layer ($\sigma_\theta > 27.8$ kg m^{-3}) across the entire Iceland Basin (5.3 ± 0.3 Sv) are taken from Johns et al. (2021). Unless otherwise noted, the uncertainties in the transports for each of the sections shown in Table 1 are either from the referenced publications or calculated for this study using the methods described in each publication.

Transports over the Iceland-Scotland Ridge are estimated from the results of Østerhus et al. (2019), Hansen et al. (2015), Hansen et al. (2016) and Berx et al. (2013), as discussed in Section 2. Østerhus et al. (2019) and Hansen et al. (2016) provide estimates of the overflow transport in the bottom layer ($\sigma_\theta > 27.8$ kg m^{-3}) to the west and east of the Faroe Islands (0.4 ± 0.3 Sv and 2.4 ± 0.2 Sv, respectively). However, there are no publications that separate the northward transport across the ridge into our upper and intermediate layers. This leaves us to determine those transports as best we can from available results. For the northward flow between Iceland and the Faroe Islands, Hansen et al. (2015) inferred a mean transport of 3.8 ± 0.5 Sv of Atlantic waters crossing the ridge ($\sigma_\theta < 27.8$ kg m^{-3}). Using a table of transport by isotherms and isohalines from their analysis (see Table 2 from Hansen et al., 2015), we estimate that 3.0 ± 0.7 Sv of this total transport contributes to the upper limb of the subpolar AMOC ($\sigma_\theta < 27.56$ kg m^{-3}), while 0.8 ± 0.3 Sv is in the intermediate layer ($27.56 < \sigma_\theta < 27.8$ kg m^{-3}). To assign the respective error estimates on these values, we proportionally distributed the total transport error from Hansen et al. (2015) and included an additional error to account for uncertainties in our interpretation of the transport distribution. For the near-surface transport between the Faroe Islands and Scotland, both Berx et al. (2013) and Østerhus et al. (2019) concluded that 2.7 ± 0.5 Sv flows northward into the Norwegian Sea. To determine this estimate, these studies used the net transport of all waters above the 5 °C isotherm and found that the maximum northward velocity was concentrated along the upper eastern continental slope near Scotland. While the North Atlantic waters near the 5 °C isotherm are below the isopycnal we are using to distinguish upper limb waters in this study, the steep temperature and salinity gradients between the upper limb waters and the overflow waters in this region make any transport in our intermediate density layer ($27.56 < \sigma_\theta < 27.8$ kg m^{-3}) minimal (see Fig. 4 from Berx et al., 2013). Therefore, this study will consider all 2.7 Sv of the northward transport between the Faroe Islands and Scotland as upper limb water ($\sigma_\theta < 27.56$ kg m^{-3}).

Summing these estimates into net inflow into the domain and net outflow from the domain results in an imbalance of 5.4 Sv, with less transport in the input (25.9 ± 1.6 Sv) than the output (31.3 ± 1.7 Sv). The above uncertainties represent standard error propagation in which all of the individual transport errors are assumed to be random and could be an underestimate of the total uncertainty if some of the transport errors are correlated. If we consider the sum of the individual errors at each section, the discrepancy of 5.4 Sv is within the overlapping uncertainties of the inflow (3.8 Sv) and outflow (4.7 Sv). Nevertheless, such a large imbalance implies that the transport estimates across some parts of the bounding sections of the domain are not representative of the average flow conditions over the nominal 4-year OSNAP period. Errors could come from measurement biases as well as the fact that some of the transports are longer-term averages based on climatological Argo/altimetry data (e.g., the flow over the Reykjanes Ridge) or compiled historical data (the flow over the Iceland-Scotland Ridge).

To attempt to resolve this transport discrepancy, we evaluated the exchanges across the OSNAP line using the OSNAP analysis, as described in Li et al. (2017). For the Iceland Basin and Rockall Trough sections, this comparison mostly resulted in changes in transport estimates of <1 Sv in each layer at each section. However, the transports over the Rockall Plateau were notably greater in the OSNAP analysis, which found nearly double the transport (8.4 Sv) for this region when compared to the glider-based estimates (4.5 Sv) from Houpert et al. (2018) (Fig. 8; Table 1). To calculate the transport in this region, the OSNAP analysis uses the available glider and Argo data across this section to estimate the geostrophic shear, and then references it to surface velocities derived from altimetry. This represents, in principle, a full four-year average over the Rockall Plateau, although the hydrographic data for the region is mostly derived from gliders. While the discrepancy between the two transport estimates is significant, the Rockall Plateau is a difficult location to continuously monitor due to its large spatial extent and complex topography, and the estimates from Houpert et al. (2018) are based solely on 19 months of intermittent glider sections. This makes these results the least robust of any of the OSNAP estimates in the eastern North Atlantic subpolar gyre since all the other estimates are from four years of continuous mooring data. If we instead use the OSNAP analysis estimate for the Rockall Plateau region, this results in a net imbalance of only 1.5 Sv over the study domain, with 29.8 ± 1.6 Sv of total inflow and 31.3 ± 1.7 Sv of total outflow. We therefore believe that the main contributing factor to the 5.4 Sv imbalance in our original estimates is due to an underestimation of North Atlantic Current flow into the domain over the Rockall-Hatton Plateau.

To try to verify this supposition using an alternative approach, we evaluated the westward transport across a meridional section through the middle of the Iceland Basin – from mooring M2 to the southeastern slope of Iceland – using Argo data (Fig. 8). Though we are only able to evaluate the top 2000 m of the water column due to the limitations of Argo data, this still includes all waters flowing through our intermediate and upper layers. Results of this analysis find that 9.6 ± 1.3 Sv of transport flows westward across this section in the upper layer and 9.5 ± 4.0 Sv flows across in the intermediate layer. This total of 19.1 Sv is slightly more than our estimated total outflow (18.6 Sv) in the upper two layers to the west (over the Reykjanes Ridge and through the East Reykjanes Ridge Current), but is well within estimated errors. Using the OSNAP analysis estimate over the Rockall Plateau also yields a very similar implied mass convergence in the upper two layers in the area east of the mid-basin Argo line, of 19.6 Sv, after subtracting the outflows across the Iceland-Scotland Ridge from the inflows across the entire NAC domain. This again suggests that our original mass budget was missing

Table 2
The mass balance estimate of transport in the eastern North Atlantic subpolar gyre as determined by this study and summarized in Fig. 9. The first row accounts for the total inflow into the region from the south and the second row accounts for the exchanges over the Iceland-Scotland Ridge. The third and fourth rows account for the density changes that occur in the eastern subpolar gyre region examined in this study. The fifth and final row is the total outflow over the Reykjanes Ridge and through the East Reykjanes Ridge Current and Iceland Scotland Overflow Water. All values in Sverdrups. Acronyms: North Atlantic Current (NAC); Iceland Scotland Overflow Water (ISOW); East Reykjanes Ridge Current (ERRC).

Transport Estimates	Upper Layer ($\sigma_\theta < 27.56$ kg m^{-3})	Intermediate Layer ($27.8 > \sigma_\theta > 27.56$)	Bottom Layer ($\sigma_\theta > 27.8$ kg m^{-3})
NAC inflow and ISOW recirculation inflow	19.4 ± 1.0	6.7 ± 1.1	0.7 ± 0.3
Outflow/inflow over Iceland-Scotland Ridge	−5.7 ± 0.9	−0.8 ± 0.3	3.3 ± 0.3
Entrainment to bottom layer	−1.4 ± 0.1	−0.6 ± 0.2	2.0 ± 0.2
Outflow over Reykjanes Ridge and through ERRC/ISOW	−6.9 ± 0.9	−11.7 ± 1.2	−6.0 ± 0.3
Implied density conversion through progressive water mass modification	−5.4 ± 1.6	6.4 ± 1.7	0.0

inflow from the North Atlantic Current along the OSNAP line to the east of mooring M2, especially since we have not yet considered potential losses from the top two layers to the bottom layer through entrainment into the Iceland Scotland Overflow Water plume upstream of the mid-basin Argo section. We will therefore use the OSNAP analysis results for the transport over the Rockall Plateau in the remainder of this study.

With our inflow and outflow estimates approximately in balance, we next attempt to calculate the overturning budget in the eastern subpolar gyre. We start with the bottom layer ($\sigma_\theta > 27.8$ kg m^{-3}). According to Johns et al. (2021), 6.0 ± 0.3 Sv of Iceland Scotland Overflow Water flows southward out of the study domain along the eastern flank of the Reykjanes Ridge, of which 0.7 ± 0.3 Sv recirculates northward back into the eastern Iceland Basin, leading to a net export of 5.3 ± 0.3 Sv from the Iceland Basin ($\sigma_\theta > 27.8$ kg m^{-3}). Of this 5.3 Sv, water mass analysis indicates that approximately 1.4 ± 0.1 Sv is derived through entrainment from the upper layer as the overflow waters descend into the Iceland Basin from the Iceland-Scotland Ridge (Table 2), and an additional 1.3 ± 0.2 Sv is entrained from the intermediate layer during the continued descent of Iceland Scotland Overflow Water into the basin. However, Johns et al. (2021) also found that approximately 0.7 ± 0.1 Sv of the dense Iceland-Scotland Ridge overflow waters were mixed upward into the intermediate layer within the southward-flowing East Reykjanes Ridge Current, implying a net vertical exchange of only 0.6 Sv from the intermediate layer to the bottom layer along the Iceland Scotland Overflow Water's pathway from the Iceland-Scotland Ridge to the OSNAP line. This implies a larger net flux of overflow waters into the basin (3.3 ± 0.3 Sv) than suggested by direct observations (2.8 ± 0.5 Sv), but both estimates are within the uncertainty of our original estimate. Given this result, we will use the larger 3.3 Sv overflow estimate from Johns et al. (2021), which reduces the overall inflow/outflow imbalance over the study domain from 1.5 Sv to 1.0 Sv. The mass budget for the bottom layer therefore indicates that 1.4 Sv of overturning occurs in the study region due to entrainment (Table 2).

Given these entrainment results from Johns et al. (2021), we can now complete our best estimate of overturning within the full study domain (Table 2 and summarized in Fig. 9). Starting with the upper layer, our analysis finds that 19.4 Sv of transport crosses the OSNAP mooring line from the south via the North Atlantic Current. Once the outflow over the Iceland-Scotland Ridge (5.7 Sv) and entrainment into Iceland Scotland Overflow Water (1.4 Sv) are subtracted, 12.3 Sv remains. Of this

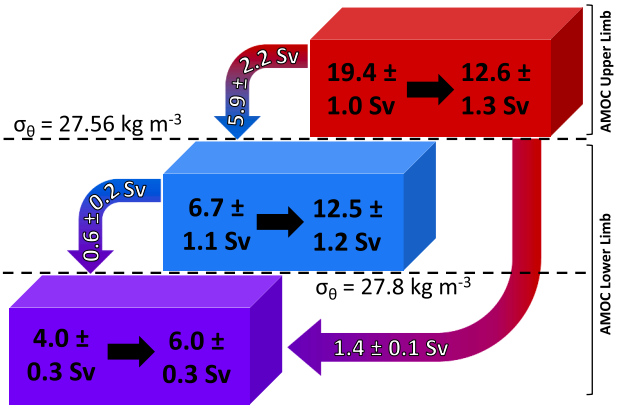

Fig. 9. Summary schematic of the overall water mass transformations occurring in the eastern North Atlantic subpolar gyre. Each box denotes the total inflow (left side of arrow) and outflow (right side of arrow) from the study domain in each potential density layer. Arrows outside the boxes denote diapycnal transfers with uncertainties. The isopycnals used to distinguish the layers are labeled and indicated by dashed lines. Overall this study finds a total of 7.3 ± 2.3 Sv of waters within the upper AMOC limb are converted to the lower limb (intermediate and deep layers) within the eastern subpolar gyre. All values in Sv.

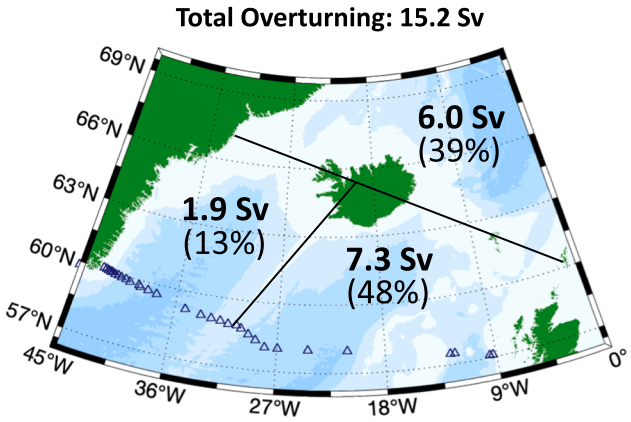

Fig. 10. Summary schematic of overturning in the northern North Atlantic and Norwegian Sea using the isopycnal of maximum overturning along the OSNAP line between Greenland and Scotland (σθ = 27.56 kg m-3). The total in the Iceland/Rockall basins (7.3 ± 2.2 Sv) is the amount determined by this study, the total in the Norwegian Sea is based on historical estimates, and the total in the Irminger Basin in the west is the amount that remains from the total overturning calculation (15.2 Sv) as determined by OSNAP. Triangles note the location of OSNAP moorings and bathymetry contours change color with every 1000 m in depth.

remaining transport, 6.9 Sv exits the region to the west through the East Reykjanes Ridge Current and across the Reykjanes Ridge. This implies that 5.4 Sv of transport is lost from the upper layer to the intermediate layer by progressive diapycnal water mass modification (i.e., overturning). Similarly for the intermediate layer, once all inflows and outflows are considered, our mass budget implies that 6.4 Sv of transport is gained from the upper layer. The difference between these two estimates is due to the residual 1 Sv mass imbalance over the study region. The error in these two density conversion estimates (±1.6 Sv for the upper layer; ±1.7 for the intermediate layer) result from standard uncertainty propagation of the transport errors for the inflows/outflows in the respective layers. Averaging these two conversions leads to a mean estimate of 5.9 ± 2.2 Sv for the overturning in the eastern subpolar gyre through progressive water mass modification, where an additional ± 0.5 Sv has been added to account for the overall 1 Sv mass imbalance. The error in this average therefore incorporates the range of possible transport estimates from the two individual calculations. While this volume of overturning seems remarkable, a previous study from Koman et al. (2020) also found an unexpected amount of overturning in a domain that is similar to our mid-basin to Reykjanes Ridge region. Their study found that the East Reykjanes Ridge Current, which covers roughly the same domain, accounts for approximately 1/3 of the total density transformation in the entire North Atlantic subpolar gyre boundary current system. Since simple thermodynamic principles dictate that warmer water cools more rapidly under similar atmospheric conditions, and that the region to the east of our mid-basin Argo section is significantly larger than the region to the west, it is likely that an even greater transformation occurs farther east due to cooling of the near-surface waters of the North Atlantic Current which are the warmest in the subpolar gyre.

In total, considering both the transformation of upper to intermediate layer waters described above, and the entrainment of upper layer waters into the dense overflows crossing the Iceland-Scotland Ridge, this analysis suggests that 7.3 ± 2.2 Sv of overturning occurs from the upper limb to the lower limb of the AMOC in the northern Iceland Basin, where the isopycnal of maximum overturning ($\sigma_\theta = 27.56$ kg m^{-3}) along the OSNAP line between Greenland and Scotland is used as the basis for defining the upper and lower AMOC limbs. From the OSNAP analysis, the 4-year mean overturning at this isopycnal across this same section from Greenland to Scotland is 15.2 Sv (Li et al., 2021). Approximately 6

Sv of this 15.2 Sv can be accounted for by transformation of upper limb waters crossing into the Norwegian Seas that return as dense overflows that cross the Greenland-Scotland Ridge, including the Iceland-Scotland overflow discussed in the background and the well-documented 3.2 Sv of dense overflow between Greenland and Iceland through the Denmark Strait (Jochumsen et al., 2017). This leaves approximately 9.2 Sv to be converted around the subpolar gyre from Scotland to Greenland, which, with our result that 7.3 Sv appears to occur in the Iceland Basin, implies that only 1.9 Sv occurs in the Irminger Basin (Fig. 10). This means that approximately 13 % of the overturning occurs in the Irminger Basin, 39 % in the Norwegian Sea, and nearly half in the subpolar gyre east of the Reykjanes Ridge. Petit et al. (2020) also found a similar estimate for the subpolar gyre overturning between the OSNAP line and the Greenland-Scotland Ridge of 7.0 ± 2.0 Sv, but did not attempt to divide it into separate contributions from the Iceland and Irminger basins. However, in considering the wintertime water mass transformations forced by air-sea buoyancy fluxes, they found that the Iceland Basin, Rockall Plateau and northern Rockall Trough are the most critical location for the pre-conditioning of the deep waters of the AMOC lower limb. Finally, it should be emphasized that the partitioning of the overturning in the different basins as described above is not representative of the actual magnitude of the density transformations occurring in each basin. The Norwegian Sea, for example, experiences a dramatic diapycnal transformation of warm, salty waters from the North Atlantic Current converting into some of the densest waters in the northern North Atlantic. The water mass changes around the subpolar gyre, on the other hand, are much more progressive and involve a lesser degree of density change as the warm near-surface waters gradually cool and sink across the overturning isopycnal.

4.3. Estimated overturning in the Irminger Basin

To attempt to validate these results, we performed an analysis of the exchanges in the Irminger Basin that is similar to the one performed in the eastern subpolar gyre. To keep the analysis simple, we only consider the upper limb ($\sigma_\theta < 27.56$ kg m^{-3}) and lower limb ($\sigma_\theta > 27.56$ kg m^{-3}) instead of the three density layers (Table 3). As previously discussed from Koman et al. (2020), the westward flow of East Reykjanes Ridge Current leakage over the Reykjanes Ridge results in an inflow into the Irminger Basin of 3.8 ± 0.8 Sv in the upper limb and 3.0 ± 1.0 Sv in the lower limb. The primary inflow into the basin is from the south through the OSNAP line via the Irminger Current. Using the results from the OSNAP analysis these contribute 3.1 Sv to the upper limb and 22.1 Sv to the lower limb. The other inflow source is from southward flow through the Denmark Strait. As previously discussed, 3.2 Sv of dense Denmark Strait Overflow Water enters the Irminger Basin at this location as part of the lower limb (Jochumsen et al., 2017), plus an additional transport of 2.0 Sv of near-surface water flows into the basin above it through the East Greenland Coastal Current and the East Greenland Current (Østerhus et al., 2019). Despite the near freezing temperatures of this 2.0 Sv, we estimate from the paper by de Steur et al. (2017; Fig. 4) that ~1.1 Sv is actually considered upper limb water due to its relative freshness (<34.5 psu), leaving ~0.9 Sv in the lower limb. The vast majority of the outflow from the Irminger Basin is southward near the tip of Greenland through the OSNAP line via the East Greenland Coastal Current and the East Greenland-Irminger Current. According to the OSNAP analysis, these flows combine to export 4.3 Sv of transport from the basin in the upper limb and 27.8 Sv of transport in the lower limb. A small additional outflow of 0.9 Sv from the Irminger Basin occurs to the north along the western Icelandic Shelf from leakage from the Irminger Current (Jónsson & Valdimarsson, 2012; Østerhus et al., 2019). Using a θ-S diagram from Jónsson & Valdimarsson (2012; Fig. 6), we estimate that ~0.5 Sv of this transport is upper limb water while the other ~0.4 is from the lower limb.

Combining these results, we find that the Irminger Basin inflow contains 8.0 Sv of transport in the upper limb of the AMOC ($\sigma_\theta < 27.56$ kg m^{-3}) and 29.2 Sv in the lower limb ($\sigma_\theta > 27.56$ kg m^{-3}) for a total inflow into the Irminger Basin of 37.2 Sv. For the waters flowing out of the basin, 4.8 Sv are in the upper limb and 28.2 are in the lower limb. This gives a total export of 33.0 Sv out of the Irminger Basin, which is 4.2 Sv less than the inflow total. This again leaves a relatively large imbalance, and it is not obvious which of the transport estimates in Table 3 is the cause of it. However, for the purposes of estimating the overturning in the Irminger Basin we can treat this imbalance in two ways. First, if we assume that all (or most) of the mass imbalance is in the lower limb transports - which seems a likely scenario since the estimated lower limb outflow from the basin is slightly less (by 1.0 Sv) than the lower limb inflow - we can arrive at an upper bound estimate of

Table 3
Estimates of transport inflow and outflow in the Irminger Basin separated by the upper (σθ < 27.56 kg m-3) and lower limbs (σθ > 27.56 kg m-3) of the AMOC as defined by the OSNAP program between Greenland and Scotland (Li et al., 2021). This budget accounts for four inflow locations and two outflow locations using transport estimates from the OSNAP analysis and recent historical estimates. To enforce mass balance, we calculated two plausible scenarios (bottom rows). In the first case (a), we attribute the entire discrepancy to the lower limb to calculate an upper bound of overturning the Irminger Basin; this results in 3.2 Sv of overturning. In the second case (b), we equally distribute the mass imbalance between the upper and lower limbs (2.1 Sv each), resulting in 1.1 Sv of overturning. All values in Sv. Acronyms: East Reykjanes Ridge Current (ERRC); Labrador Sea Water (LSW); Denmark Strait Overflow Water (DSOW); East Greenland Coastal Current (EGCC); East Greenland Current (EGC); East Greenland-Irminger Current (EGIC). Uncertainties are based on calculated errors from the OSNAP analysis, published results in Østerhus et al. (2019) and Jochumsen et al. (2012), estimates from de Steur et al. (2017) and Jónsson & Valdimarsson (2012), and, where relevant, the proper propagation of errors.

INFLOW:	Upper Limb ($\sigma_\theta < 27.56$ kg m^{-3})	Lower Limb ($\sigma_\theta > 27.56$ kg m^{-3})	Total
ERRC leakage over Reykjanes Ridge	3.8 ± 0.8	3.0 ± 1.0	6.8 ± 1.3
Irminger Current	3.1 ± 0.3	22.1 ± 0.7	25.2 ± 0.8
DSOW through Denmark Strait		3.2 ± 0.1	3.2 ± 0.1
EGCC/EGC over Denmark Strait	1.1 ± 0.5	0.9 ± 0.4	2.0 ± 0.5
Total Inflow:	**8.0 ± 1.0**	**29.2 ± 1.3**	**37.2 ± 1.6**
OUTFLOW:			
Irminger Current leakage over the Western Icelandic Shelf	0.5 ± 0.2	0.4 ± 0.2	0.9 ± 0.1
EGCC/EGIC	4.3 ± 0.3	27.8 ± 0.5	32.1 ± 0.6
Total Outflow:	**4.8 ± 0.4**	**28.2 + 0.5**	**33.0 ± 0.7**
Overall gain/loss between inflow and outflow	−3.2	−1.0	−4.2
WITH ENFORCED MASS BALANCE:			
Net inflow	8.0[a] (5.9)[b]	29.2[a] (29.2) [b]	37.2[a] (35.1) [b]
Net outflow	4.8[a] (4.8) [b]	33.4[a] (30.3) [b]	37.2[a] (35.1) [b]
Overall gain/loss between inflow and outflow	−3.2[a] (-1.1) [b]	3.2[a] (1.1) [b]	0.0[a] (0.0)[b]

the overturning of 3.2 Sv, which is simply the difference of the upper layer inflow (8.0 Sv) and upper layer outflow (4.8 Sv) from the basin. Alternatively, if we split the 4.2 Sv mass imbalance equally between the upper and lower layers, so that the upper layer net inflow is decreased by 2.1 Sv and the lower layer outflow is increased by 2.1 Sv, this results in an overturning estimate of 1.1 Sv for the Irminger Basin (Table 3). The midpoint of these two estimates is very close to the 1.9 Sv estimate implied from our earlier analysis of the Iceland Basin, and suggests that the overturning in the Irminger Basin is not likely to be more than about 3 Sv. These results support our conclusion that the Iceland Basin is the dominant region of overturning in the northern subpolar gyre mostly due to progressive water mass modification.

Finally, we note that these results are not highly sensitive to the specific choice of density interface between the upper and lower AMOC limbs. If the isopycnal of maximum overturning for the full OSNAP array including the Labrador Sea (σ_θ = 27.66 kg m^{-3}) is used, instead of the isopycnal of maximum overturning across the Greenland-Scotland portion of the array (σ_θ = 27.56 kg m^{-3}), the results for the overturning in the Irminger Basin are identical. The upper bound estimate for overturning in the basin would remain at 3.2 Sv, and an equal distribution of the mass balance discrepancy between the two limbs would likewise result in only 1.1 Sv of overturning. On the other hand, using this denser isopycnal for the region to the east of the Reykjanes Ridge does reduce the overturning estimate by 1.0 Sv (7.3 to 6.3 Sv), but this value is still well within the error of our Iceland Basin overturning estimate (±2.2 Sv).

5. Summary and conclusions

The North Atlantic Current is the primary conduit of the upper limb of the AMOC as it enters the North Atlantic subpolar gyre through the Iceland Basin, over the Rockall Plateau, and through the Rockall Trough. We estimate that the total transport of the North Atlantic Current entering through these locations is ~25–27 Sv (σ_θ < 27.8 kg m^{-3}), with 13–14 Sv flowing through the Iceland Basin, ~4–5 Sv entering through the Rockall Trough, and ~8–9 Sv flowing over the Rockall Plateau primarily through the Hatton Bank Jet and the Rockall Bank Jet. We further find that approximately 19–20 Sv of the North Atlantic Current transports waters within the upper limb of the AMOC (σ_θ < 27.56 kg m^{-3}), including ~7–8 Sv in the Iceland Basin, ~5 in the Rockall Trough, and about 7 Sv over the Rockall Plateau. This agrees with the range (16–20 Sv) of estimated North Atlantic Current inflow in the upper AMOC limb from previous studies (Daniault et al., 2016; Mercier et al., 2015; Sarafanov et al., 2012). Our results also suggest that <20 % of the subpolar gyre inflow from the North Atlantic Current enters the Rockall Trough, while over 80 % enters through the Iceland Basin and over the Rockall Plateau. While this ratio is not as extreme as the 10 %/90 % breakdown suggested by Bower et al. (2019), it confirms that the vast majority of North Atlantic Current inflow occurs to the west of the Rockall Trough.

Within the Iceland Basin, our analysis finds that the North Atlantic Current enters the region as a primary flow on the eastern side of the basin near 23.5°W with a mostly barotropic, secondary flow in the middle of the basin near 26°W. Through westward eddy propagation and meanders of the primary branch, these two conduits of the North Atlantic Current regularly interact resulting in a strong negative correlation between them. In certain cases, this even results in the primary branch intermittently occupying the location of the secondary branch. Results from Argo and altimetry data compare favorably and agree closely on the mean transports, velocities, and locations of the North Atlantic Current branches. The altimetry-based time series also reveals that much of the North Atlantic Current's variability is due to the barotropic component of the transport, while water mass analysis from Argo finds that both branches likely contain more recirculated subpolar gyre water than subtropical-origin water due to their relative freshness (<35.15 psu).

An important result from this study is the determination that 7.3 ± 2.3 Sv of the AMOC occurs in the North Atlantic subpolar gyre to the east of the Reykjanes Ridge. This includes 1.4 ± 0.1 Sv of overturning due to the entrainment of upper AMOC limb waters into the Norwegian Sea Overflows descending into the Iceland Basin, and 5.9 ± 2.2 Sv from progressive water mass modification through buoyancy loss. It should be noted that if we calculate overturning using the original mass budget of the eastern subpolar gyre, which has a mass imbalance of 5.4 Sv, and apply the proportional redistribution method described in the Irminger Basin section, the estimated overturning 6.2 Sv. While this value is ~1 Sv lower than our final overturning calculation, it still suggests the eastern subpolar gyre has more overturning than any other region. If, additionally, we assume that the 1.9 Sv of overturning that we estimate to occur in the Irminger Basin is entirely due to progressive water mass transformation, we obtain a total of 7.8 Sv for the total buoyancy-forced overturning over the subpolar gyre between the OSNAP line and the Greenland-Scotland Ridge. This is consistent with the recent study by Petit et al. (2020) which found a value of 7.0 ± 2.5 Sv for the overturning due to buoyancy forcing over this same region. It is unlikely that very much, if any, of the overturning in the Irminger basin is due to entrainment into the Denmark Strait overflow, since previous studies suggest that the entrainment into that overflow is all drawn from waters already within the lower limb (σ_θ > 27.56 kg m^{-3}; Tanhua et al., 2005). Our results therefore agree with Petit et al. (2020) that entrainment into the deep overflows does not play a major role in the transformation of upper limb water to the lower limb, as it only accounts for O(1.5 Sv) of the 9.2 Sv of total overturning across this region.

This study concludes that nearly half of the AMOC occurs to the east of the Reykjanes Ridge between the OSNAP line and the Iceland-Scotland Ridge. Given that previous studies have noted that the waters in the Rockall Trough propagate directly to the Norwegian Sea (Holliday et al., 2008), and that virtually all the water entering the Norwegian Sea from the Rockall Trough is at densities within the upper limb (Fig. 8), it is likely that the vast majority of the overturning in this region is isolated to the domain of the Rockall Plateau and Iceland Basin. These results are based on a collection of estimates covering different time periods with different averaging time scales, and more studies will be needed to further substantiate these results. However, with the recent revelation that little overturning occurs in the Labrador Basin (Lozier et al., 2019), this study provides evidence that much of the upper to deep limb water mass transformation of the AMOC in the subpolar North Atlantic occurs in the northern Iceland Basin.

Declaration of Competing Interest

The authors declare that they have no known competing financial interests or personal relationships that could have appeared to influence the work reported in this paper.

Acknowledgements

The authors would like to thank the captains and crews of the R/V Knorr, R/V Pelagia, RRS Discovery and R/V Neil Armstrong for their hospitality aboard their vessels and for helping to ensure the completion of this research. We would also like to recognize the North Atlantic Observed Climatological Mean Absolute Geostrophic Velocity Profiles data base in the University of Miami's Scholarly Repository which was used for much of the mean Argo velocity data in this study. This data can be accessed at https://scholarlyrepository.miami.edu/ocean_sciences_supp/8/. OSNAP data used in this study is available at https://www.o-snap.org/oberservations/data/. Finally, we would like to thank the National Science Foundation for funding this research through grants OCE-1259398, OCE-1756231, OCE-1948335, and OCE-1948505.

References

Bacon, S., 1997. Circulation and fluxes in the North Atlantic between Greenland and Ireland. J. Phys. Oceanogr. 27(7), 1420–1435. https://doi.org/10.1175/1520-0485(1997)027<1420:CAFITN>2.0.CO;2.

Beaird, N.L., Rhines, P.B., Eriksen, C.C., Beaird, N.L., Rhines, P.B., Eriksen, C.C., 2013. Overflow waters at the Iceland-Faroe Ridge observed in multiyear seaglider surveys. J. Phys. Oceanogr. 43 (11), 2334–2351. https://doi.org/10.1175/JPO-D-13-029.1.

Berx, B., Hansen, B., Østerhus, S., Larsen, K.M., Sherwin, T., Jochumsen, K., 2013. Combining in situ measurements and altimetry to estimate volume, heat and salt transport variability through the Faroe-Shetland Channel. Ocean Sci. 9, 639–654. https://doi.org/10.5194/os-9-639-2013.

Bilo, T.C., 2019. North Atlantic observed climatological mean absolute geostrophic velocity profiles. University of Miami Libraries. https://doi.org/10.17604/cf5z-x124.

Bilo, T.C., Johns, W.E., 2019. Interior pathways of Labrador sea water in the north Atlantic from the Argo perspective. Geophys. Res. Lett. 46 (6), 3340–3348. https://doi.org/10.1029/2018GL081439.

Bower, A., Furey, H., 2017. Iceland-Scotland overflow water transport variability through the Charlie-Gibbs fracture Zone and the impact of the North Atlantic Current. J. Geophys. Res. Oceans 122, 6989–7012. https://doi.org/10.1002/2017JC012698.

Bower, A.S., Le Cann, B., Rossby, T., Zenk, W., Gould, J., Speer, K., Richardson, P.L., Prater, M.D., Zhang, H.-M., 2002. Directly measured mid-depth circulation in the northeaster North Atlantic Ocean. Nature 419. https://doi.org/10.1038/nature01106.

Bower, A., Lozier, S., Biastoch, A., Drouin, K., Foukal, N., Furey, H., Lankhorst, M., Rühs, S., Zou, S., 2019. Lagrangian views of the pathways of the Atlantic Meridional Overturning Circulation. J. Geophys. Res. Oceans 124, 5313–5335. https://doi.org/10.1029/2019JC015014.

Brambilla, E., Talley, L.D., 2008. Subpolar mode water in the northeastern Atlantic: 1. Averaged properties and mean circulation. J. Geophys. Res. 113, C04025. https://doi.org/10.1029/2006JC004062.

Chafik, L., Rossby, T., Schrum, C., 2014. On the spatial structure and temporal variability of poleward transport between Scotland and Greenland. J. Geophys. Res. Oceans 119 (2), 824–841. https://doi.org/10.1002/2013JC009287.

Daniault, N., Mercier, H., Lherminier, P., Sarafanov, A., Falina, A., Zunino, P., Pérez, F.F., Ríos, A.F., Ferron, B., Huck, T., Thierry, V., Gladyshev, S., 2016. The northern North Atlantic Ocean mean circulation in the early 21st century. Prog. Oceanogr. 146, 142–158. https://doi.org/10.1016/J.POCEAN.2016.06.007.

de Steur, L., Pickart, R.S., Macrander, A., Våge, K., Harden, B., Jónsson, S., Østerhus, S., Valdimarsson, H., 2017. Liquid freshwater transport estimates from the East Greenland Current based on continuous measurements north of Denmark Strait. J. Geophys. Res. Oceans 122, 93–109. https://doi.org/10.1002/2016JC012106.

Dickson, R., Brown, J., 1994. The production of North Atlantic Deep Water: sources, rates, and pathways. J. Geophys. Res. 99 (C6), 12319–12341. https://doi.org/10.1029/94JC00530.

Fogelqvist, E., Blindheim, J., Tanhua, T., Østerhus, S., Buch, E., Rey, F., 2003. Greenland-Scotland overflow studied by hydro-chemical multivariate analysis. Deep-Sea Research Part I: Oceanogr. Res. Pap. 50, 73–102. https://doi.org/10.1016/S0967-0637(02)00131-0.

Fratantoni, D.M., 2001. North Atlantic surface circulation during the 1990s observed with satellite-tracked drifters. J. Geophys. Res. 106 (C10), 22067–22093. https://doi.org/10.1029/2000JC000730.

Hansen, B., Østerhus, S., 2000. North Atlantic-Nordic Seas exchanges. Prog. Oceanogr.. Pergamon. 45 (2), 109–208.

Hansen, B., Larsen, K.M.H., Olsen, S.M., Quadfasel, D., Jochumsen, K., Østerhus, S., 2018. Overflow of cold water across the Iceland-Faroe Ridge through the Western Valley. Ocean Sci. 14, 871–885. https://doi.org/10.5194/os-14-871-2018.

Hansen, B., Østerhus, S., 2007. Faroe Bank Channel overflow 1995–2005. Prog. Oceanogr. 75, 817–856. https://doi.org/10.1016/j.pocean.2007.09.004.

Hansen, B., Larsen, K.M.H., Hátún, H., Kristiansen, R., Mortensen, E., Østerhus, S., 2015. Transport of volume, heat, and salt towards the Arctic in the Faroe Current 1993–2013. Ocean Sci. 11, 743–757. https://doi.org/10.5194/os-11-743-2015.

Hansen, B., Húsgarð Larsen, K.M., Hátún, H., Østerhus, S., 2016. A stable Faroe Bank Channel overflow 1995–2015. Ocean Sci. 12, 1205–1220. https://doi.org/10.5194/os-12-1205-2016.

Harvey, J.G., Theodorou, A., 1986. The circulation of Norwegian Sea overflow water in the eastern North Atlantic. Oceanol. Acta 9, 393–402.

Hermann, F., 1967. The T–S diagram analysis of the water masses over the Iceland–Faroe Ridge and in the Faroe Bank Channel (Overflow '60), Rapport et Procé-Verbaux Reunion Conseil Internationale Exploration de La Mer, 157, 139–149.

Heywood, K.J., McDonagh, E.L., White, M.A., 1994. Eddy kinetic energy of the North Atlantic subpolar gyre from satellite altimetry. J. Geophys. Res. 99 (C11), 22525. https://doi.org/10.1029/94JC01740.

Holliday, N.P., Pollard, R.T., Read, J.F., Leach, H., 2000. Water mass properties and fluxes in the Rockall Trough, 1975–1998. Deep Sea Res. Part I 47 (7), 1303–1332. https://doi.org/10.1016/S0967-0637(99)00109-0.

Holliday, N.P., Hughes, S.L., Bacon, S., Beszczynska-Möller, A., Hansen, B., Lavín, A., Loeng, H., Mork, K.A., Østerhus, S., Sherwin, T., Walczowski, W., 2008. Reversal of the 1960s to 1990s freshening trend in the northeast North Atlantic and Nordic Seas. Geophys. Res. Lett. 35 (3).

Holliday, N.P., Cunningham, S.A., Johnson, C., Gary, S.F., Griffiths, C., Read, J.F., Sherwin, T., 2015. Multidecadal variability of potential temperature, salinity, and transport in the eastern subpolar North Atlantic. J. Geophys. Res. Oceans 120 (9), 5945–5967. https://doi.org/10.1002/2015JC010762.

Houpert, L., Cunningham, S., Fraser, N., Johnson, C., Holliday, N.P., Jones, S., Moat, B., Rayner, D., 2020. Observed variability of the North Atlantic Current in the Rockall Trough from 4 years of mooring measurements. J. Geophys. Res.: Oceans, 125(10), e2020JC016403. https://doi.org/10.1029/2020JC016403.

Houpert, L., Inall, M.E., Dumont, E., Gary, S., Johnson, C., Porter, M., Johns, W.E., Cunningham, S.A., 2018. Structure and Transport of the North Atlantic Current in the Eastern Subpolar Gyre from Sustained Glider Observations. J. Geophys. Res. Oceans 123 (8), 6019–6038. https://doi.org/10.1029/2018JC014162.

Hughes, S.L., Turrell, W.R., Hansen, B., Østerhus, S., 2006. Fluxes of Atlantic Water (Volume, Heat and Salt) in the Faroe-Shetland Channel Calculated from a Decade of Acoustic Doppler Current Profiler Data (1994–2005), available at: http://www.scotland.gov.uk/Uploads/Documents/Coll0106.pdf.

Jochumsen, K., Quadfasel, D., Valdimarsson, H., Jónsson, S., 2012. Variability of the Denmark Strait overflow: Moored time series from 1996–2011. J. Geophys. Res. Oceans 117 (C12), n/a–n/a.

Jochumsen, K., Moritz, M., Nunes, N., Quadfasel, D., Larsen, K.M.H., Hansen, B., Valdimarsson, H., Jónsson, S., 2017. Revised transport estimates of the Denmark Strait overflow. J. Geophys. Res. Oceans 122, 3434–3450. https://doi.org/10.1002/2017jc012803.

Johns, W.E., Devana, M., Houk, A., Zou, S., 2021. Moored observations of the Iceland-Scotland Overflow plume along the eastern flank of the Reykjanes Ridge. J. Geophys. Res. Oceans 126 (8). https://doi.org/10.1029/2021JC017524.

Johnson, C., Sherwin, T., Cunningham, S., Dumont, E., Houpert, L., Holliday, N.P., 2017. Transports and pathways of overflow water in the Rockall Trough. Deep-Sea Research Part I 122, 48–59. https://doi.org/10.1016/j.dsr.2017.02.004.

Jónsson, S., Valdimarsson, H., 2012. Water mass transport variability to the North Icelandic shelf, 1994–2010. ICES J. Mar. Sci. 69, 809–815. https://doi.org/10.1093/icesjms/fss024.

Kanzow, T., Zenk, W., 2014. Structure and transport of the Iceland Scotland Overflow plume along the Reykjanes Ridge in the Iceland Basin. Deep Sea Res. Part I 86, 82–93. https://doi.org/10.1016/J.DSR.2013.11.003.

Knutsen, Ø., Svendsen, H., Østerhus, S., Rossby, T., Hansen, B., 2005. Direct measurements of the mean flow and eddy kinetic energy structure of the upper ocean circulation in the NE Atlantic. Geophys. Res. Lett. 32 (14), n/a-n/a. https://doi.org/10.1029/2005GL023615.

Koman, G., Johns, W.E., Houk, A., 2020. Transport and evolution of the East Reykjanes Ridge Current. J. Geophys. Res. Oceans 125 (10). https://doi.org/10.1029/2020JC016377.

Krauss, W., 1995. Current and mixing in the Irminger Sea and in the Iceland Basin. J. Geophys. Res. 100, 10851–10871. https://doi.org/10.1029/95JC00423.

Lebedev, K.V, Yoshinari, H., Maximenko, N.A., Hacker, P.W., 2007. YoMaHa'07: Velocity data assessed from trajectories of Argo floats at parking level and at the sea surface. Retrieved from http://apdrc.soest.hawaii.edu/projects/yomaha/yomaha07/YoMaHa070612small.pdf.

Lherminier, P., Mercier, H., Huck, T., Gourcuff, C., Perez, F.F., Morin, P., Sarafanov, A., Falina, A., 2010. The Atlantic Meridional Overturning Circulation and the subpolar gyre observed at the A25-OVIDE section in June 2002 and 2004. Deep Sea Res. Part I 57 (11), 1374–1391. https://doi.org/10.1016/J.DSR.2010.07.009.

Li, F., Lozier, M.S., Bacon, S., Bower, A., Cunningham, S.A., de Jong, M.F., DeYoung, B., Fraser, N., Fried, N., Holliday, N. P., Holte, J., Houpert, L., Inall, M.E., Johns, W.E., Jones, S., Johnson, C., Karstensen, J., LeBras, I.A., Lherminier, P., Lin, X., Mercier, H., Oltmanns, M., Pacini, A., Pickart, R.S., Rayner, D., Straneo, F., Thierry, V., Visbeck, M., Yashayaev, I., & Zhou, C. (2021). Subpolar North Atlantic western boundary density anomalies and the Meridional Overturning Circulation. *Nature Communications*, **12**, 3002 (2021). https://doi.org/10.1038/s41467-021-23350-2.

Li, F., Lozier, M.S., Johns, W.E., 2017. Calculating the meridional volume, heat and freshwater transports from an observing system in the subpolar North Atlantic: observing system simulation experiment. J. Atmos. Oceanic Technol. 34, 1483–1500. https://doi.org/10.1175/JTECH-D-16-0247.1.

Lozier, M.S., Bacon, S., Bower, A.S., Cunningham, S.A., de Jong, M.F., de Steur, L., de Young, B., Fischer, J., Gary, S.F., Greenan, B.J.W., Heimbach, P., Holliday, N.P., Houpert, L., Inall, M.E., Johns, W.E., Johnson, H.L., Karstensen, J., Li, F., Lin, X., Mackay, N., Marshall, D.P., Mercier, H., Myers, P.G., Pickart, R.S., Pillar, H.R., Straneo, F., Thierry, V., Williams, R.G., Wilson, C., Yang, J., Zhao, J., Zika, J.D., 2017. Overturning in the Subpolar North Atlantic Program: a new international ocean observing system. Bull. Am. Meteorol. Soc. 98 (4), 737–752. https://doi.org/10.1175/BAMS-D-16-0057.1.

Lozier, M.S., Li, F., Bacon, S., Bahr, F., Bower, A.S., Cunningham, S.A., de Jong, M.F., de Steur, L., de Young, B., Fischer, J., Gary, S.F., Greenan, B.J.W., Holliday, N.P., Houk, A., Houpert, L., Inall, M.E., Johns, W.E., Johnson, H.L., Johnson, C., Karstensen, J., Koman, G., le Bras, I.A., Lin, X., Mackay, N., Marshall, D.P., Mercier, H., Oltmanns, M., Pickart, R.S., Ramsey, A.L., Rayner, D., Straneo, F., Thierry, V., Torres, D.J., Williams, R.G., Wilson, C., Yang, J., Yashayaev, I., Zhao, J., 2019. A sea change in our view of overturning in the subpolar North Atlantic. Science 363 (6426), 516–521. https://doi.org/10.1126/science.aau6592.

Martin, A.P., Wade, I.P., Richards, K.J., Heywood, K.J., 1998. The PRIME eddy. Journal of Marine Research, 56, 439-462. https://doi.org/10.1357/002224098321822375.

Mercier, H., Lherminier, P., Sarafanov, A., Gaillard, F., Daniault, N., Desbruyères, D., Falina, A., Ferron, B., Gourcuff, C., Huck, T., Thierry, V., 2015. Variability of the meridional overturning circulation at the Greenland-Portugal OVIDE section from 1993 to 2010. Prog. Oceanogr. 132, 250–261. https://doi.org/10.1016/J.POCEAN.2013.11.001.

Olsen, S.M., Hansen, B., Østerhus, S., Quadfasel, D., Valdimarsson, H., 2016. Biased thermohaline exchanges with the Arctic across the Iceland-Faroe Ridge in ocean climate models. Ocean Sci. 12, 545–560. https://doi.org/10.5194/os-12-545-2016.

Olson, S.M., Hansen, B., Quadfasel, D., Østerhus, S., 2008. Observed and modelled stability of overflow across the Greenland-Scotland ridge. Nature 455, 519–522. https://doi.org/10.1038/nature07302.

Østerhus, S., Sherwin, T., Quadfasel, D., Hansen, B., 2008. In: Arctic–Subarctic Ocean Fluxes. Springer Netherlands, Dordrecht, pp. 427–441.

Østerhus, S., Woodgate, R., Valdimarsson, H., Turrell, B., de Steur, L., Quadfasel, D., Olsen, S.M., Moritz, M., Lee, C.M., Larsen, K.M.H., Jónsson, S., Johnson, C., Jochumsen, K., Hansen, B., Curry, B., Cunningham, S., Berx, B., 2019. Arctic Mediterranean exchanges: a consistent volume budget and trends in transports from two decades of observations. Ocean Sci. 15 (2), 379–399. https://doi.org/10.5194/os-15-379-2019.

Paillet, J., Mercier, H., 1997. An inverse model of the eastern North Atlantic general circulation and thermocline ventilation. Deep-Sea Research Part I 44, 1293–1328. https://doi.org/10.1016/S0967-0637(97)00019-8.

Perkins, H., Hopkins, T.S., Malmberg, S.A., Poulain, P.M., Warn-Varnas, A., 1998. Oceanographic conditions east of Iceland. J. Geophys. Res. Oceans 103, 21531–21542. https://doi.org/10.1029/98JC00890.

Petit, T., Mercier, H., Thierry, V., 2019. New insight into the formation and evolution of the East Reykjanes Ridge Current and Irminger Current. J. Geophys. Res. Oceans 124 (12), 9171–9189. https://doi.org/10.1029/2019JC015546.

Petit, T., Lozier, S., Josey, S.A., Cunningham, S., 2020. Atlantic deep water formation occurs primarily in the iceland basin and irminger sea by local buoyancy forcing. Geophys. Res. Lett. 47 (22) https://doi.org/10.1029/2020GL091028.

Pujol, M.-I.-I., Faugère, Y., Taburet, G., Dupuy, S., Pelloquin, C., Ablain, M., Picot, N., 2016. DUACS DT2014: The new multi-mission altimeter data set reprocessed over 20 years. Ocean Sci. 12 (5), 1067–1090. https://doi.org/10.5194/os-12-1067-2016.

Quadfasel, D., Käse, R., 2007. Present-Day Manifestation of the Nordic Seas Overflows. In: Schmittner, A., Chiang, J.C.H., Hemming, S.R. (Eds.), Ocean Circulation: Mechanisms and Impacts. American Geophysical Union, Washington, D.C., pp. 75–89. https://doi.org/10.1029/173GM07

Read, J.F., Pollard, R.T., 2001. A long-lived eddy in the Iceland Basin 1998. J. Geophys. Res. Oceans 106 (C6), 11411–11421. https://doi.org/10.1029/2000JC000492.

Roemmich, D., Gilson, J., 2009. The 2004–2008 mean and annual cycle of temperature, salinity, and steric height in the global ocean from the Argo Program. Prog. Oceanogr. 82 (2), 81–100. https://doi.org/10.1016/J.POCEAN.2009.03.004.

Roessler, A., Rhein, M., Kieke, D., Mertens, C., 2015. Long-term observations of North Atlantic Current transport at the gateway between western and eastern Atlantic: NAC transport observations at MAR. Journal of Geophysical Research: Oceans, 120, 4003–4027. https://doi.org/10.1002/2014JC010662.

Rossby, T., Prater, M.D., Zhang, H.-M., Anderson-Fontana, S., Perez-Brunius, P., Lazarevich, P., Bower, A.S., Richardson, P.L., Hunt, H.D., 2000. Warm-water pathways in the Subpolar North Atlantic: Some case studies. International WOCE News, 38, 17–19. Retrieved from https://www.scopus.com/record/display.uri?eid=2-s2.0-0004053416&origin=inward&txGid=3acd4487dcbeba87a75cd8dbba17e0e9.

Rossby, T., Prater, M.D., Søiland, H., 2009. Pathways of inflow and dispersion of warm waters in the Nordic seas. J. Geophys. Res. 114, C04011. https://doi.org/10.1029/2008JC005073.

Rossby, T., Flagg, C., Chafik, L., Harden, B., Søiland, H., 2018. A direct estimate of volume, heat, and freshwater exchange across the Greenland-Iceland-Faroe-Scotland Ridge. J. Geophys. Res. Oceans 123, 7139–7153. https://doi.org/10.1029/2018JC014250.

Sarafanov, A., Falina, A., Mercier, H., Sokov, A., Lherminier, P., Gourcuff, C., Gladyshev, S., Gaillard, F., Daniault, N., 2012. Mean full-depth summer circulation and transports at the northern periphery of the Atlantic Ocean in the 2000s. J. Geophys. Res. Oceans 117 (C1). https://doi.org/10.1029/2011JC007572.

Saunders, P.M., 1994. The flux of overflow water through the Charlie-Gibbs Fracture Zone. J. Geophys. Res. 99 (C6), 12343. https://doi.org/10.1029/94JC00527.

Saunders, P.M., 1996. The flux of dense cold overflow water southeast of Iceland. J. Phys. Oceanogr. 26, 85–95. https://doi.org/10.1175/1520-0485(1996)026<0085:TFODCO>2.0.CO;2.

Sherwin, T.J., Griffiths, C.R., Inall, M.E., Turrell, W.R., 2008. Quantifying the overflow across the Wyville Thomson Ridge into the Rockall Trough. Deep-Sea Research Part I 55, 396–404. https://doi.org/10.1016/j.dsr.2007.12.006.

Shoosmith, D.R., Richardson, P.L., Bower, A.S., Rossby, H.T., 2005. Discrete eddies in the northern North Atlantic as observed by looping RAFOS floats. Deep Sea Res. Part II 52 (3–4), 627–650. https://doi.org/10.1016/J.DSR2.2004.12.011.

Sy, A., Schauer, U., Meincke, J., 1992. The North-Atlantic Current and its associated hydrographic structure above and eastwards of the Mid-Atlantic Ridge. Deep-Sea Res. 39 (5), 825–853.

Tanhua, T., Olsson, K.A., Jeansson, E., 2005. Formation of Denmark Strait overflow water and its hydro-chemical composition. J. Mar. Syst. 57 (3-4), 264–288.

Treguier, A. M., Theetten, S., Chassignet, E. P., Penduff, T., Smith, R., Talley, L., Beismann, J.O., Böning, C., 2005. The North Atlantic subpolar gyre in four high-resolution models. J. Phys. Oceanogr. Retrieved from https://journals.ametsoc.org/doi/pdf/10.1175/JPO2720.1.

Turrell, W.R., Hansen, B., Østerhus, S., Hughes, S.L., Ewart, K., Hamilton, J., 1999. Direct observatons of inflow to the Nordic Seas through the Faroe Shetland Channel 1994–1998. ICES J. Mar. Sci. CM1999/L:01.

van Aken, H.M., Becker, G., 1996. Hydrography and through-flow in the north-eastern North Atlantic Ocean: the NANSEN project. Prog. Oceanogr. 38 (4), 297–346. https://doi.org/10.1016/S0079-6611(97)00005-0.

Voet, G., 2010. On the Nordic Overturning Circulation, Dissertation zur Erlangung des Doktorgrades der Naturwissenschaften im Fachbereich Geowissenschaften der Universität Hamburg, Hamburg, 98 pp.

Wade, I.P., Heywood, K.J., 2001. Tracking the PRIME eddy using satellite altimetry. Deep Sea Res. Part II 48 (4–5), 725–737. https://doi.org/10.1016/S0967-0645(00)00094-1.

Xu, X., Schmitz, W.J., Hurlburt, H.E., Hogan, P.J., Chassignet, E.P., 2010. Transport of Nordic Seas overflow water into and within the Irminger Sea: an eddy-resolving simulation and observations. J. Geophys. Res. 115, C12048. https://doi.org/10.1029/2010JC006351.

Zhao, J., Bower, A., Yang, J., Lin, X., Zhou, C., 2018. Structure and formation of anticyclonic eddies in the Iceland Basin. J. Geophys. Res. Oceans 123 (8), 5341–5359. https://doi.org/10.1029/2018JC013886.